Consortium for Small-Scale Modelling

Newsletter

June 2016 *No. 16*

Deutscher Wetterdienst

Ufficio Generale Spazio Aereo e Meteorologia

Instytucie Meteorogii i Gospodarki Wodnej

Agenzia Regionale per la Protezione Ambientale dell'Emilia Romagna Servizio Idro Meteo Clima

Centro Italiano Ricerche Aerospaziali

MeteoSwiss

ΕΘΝΙΚΗ ΜΕΤΕΩΡΟΛΟΓΙΚΗ ΥΠΗΡΕΣΙΑ

Administratia Nationala de Meteorologie

Federal Service for Hydrometeorology and Environmental Monitoring

Amt fur GeoInformationswesen der Bundeswehr

Agenzia Regionale per la Protezione Ambientale del Piemonte

www.cosmo-model.org

Editors: Mihaela Bogdan (NMA); Massimo Milelli (ARPA-Piedmont); Ulrich Schattler (DWD);

Table of Contents

The current issue of the COSMO Newsletter presents examples of the recent developments within the COSMO consortium. I would like to very much thank the authors for sharing their results and to strongly encourage all COSMO Scientists to use the Newsletter for presentation of your results.

The recent progress within the consortium was extensively reviewed and discussed during the COSMO General Meeting held from 7 to 10 September 2015 in Wrocław, Poland. You can find the GM presentations at *http://www.cosmo-model.org/content/consortium/generalMeetings/general2015/default.htm*

The newly implemented COSMO Science Plan guides further developments within our consortium and focuses them very much on convection-permitting ensemble NWP methods. The developments are (directly and indirectly) supported by many current COSMO Priority Projects and Tasks, covering scientific areas from EPS methodology to assimilation, physics, verification and software engineering. In result, the COSMO convection-scale ensembles are now close to operational implementation in Switzerland and under development in other COSMO countries, not to mention the very first such operational system already working at DWD. The DWD and MeteoSwiss ensembles were recently tested by European Severe Storm Laboratory. The evaluation shown significant skill of the tools and indicated some areas for further development, including e.g. convection initiation. I would like to thank and express my gratitude to all COSMO Scientists who participate in the work of the consortium and to encourage your further active involvement in the COSMO work. There is still a lot to be done!

For the next General Meeting, we will meet in Offenbach, Germany, from 5 to 8 September 2016. I wish every success in your work!

Michał Ziemiański
COSMO Scientific Project Manager

Figure 1: Participants of the 16th COSMO General Meeting in Polonia

Urban heat island effects over Torino

M. Milelli [1]

[1] *ARPA Piemonte*

1 Introduction

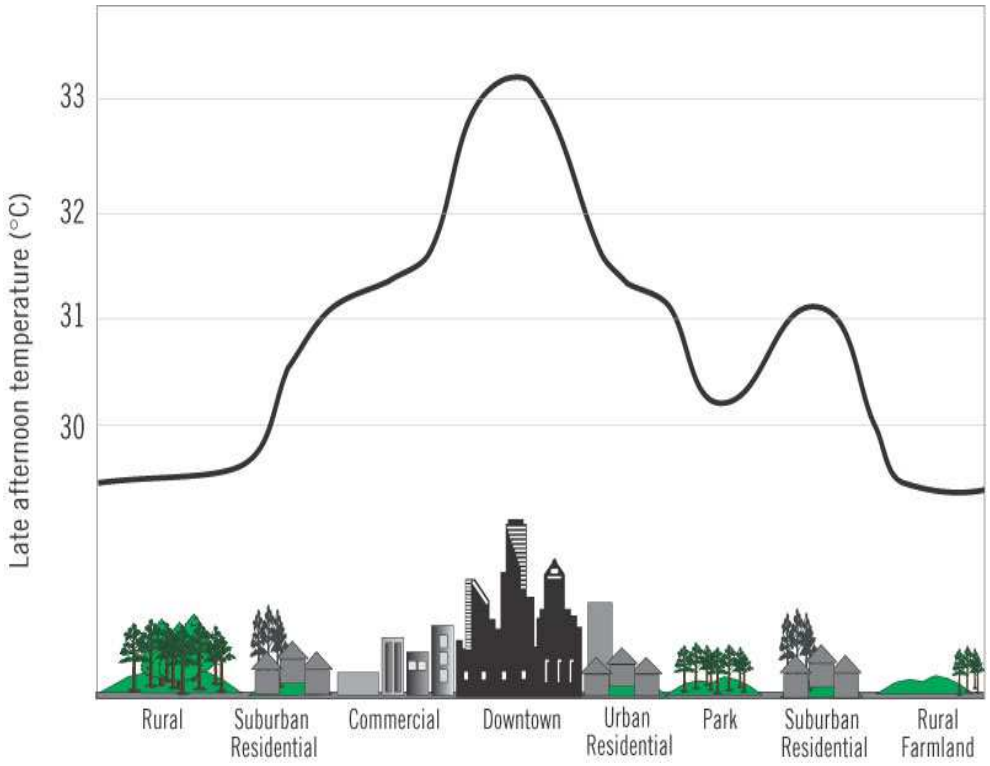

Figure 1: Urban heat island generalized scheme (source: EPA).

The increase of built surfaces (with consequent reduction of natural surfaces) constitutes the main reason for the formation of UHIs. While natural soil with vegetation uses most of the absorbed radiation in evapotranspiration processes with release of water vapor cooling the surrounding air, paved terrains and buildings tend to absorb a lot of the incident radiation which is then released as heat. The presence of parks in the city has a beneficial effect because of horizontal air circulation due to the formation of temperature gradients. Instead, urban canyons block the release of the reflected radiation. So the main characteristics of UHIs are the following:

- during the warmest hours of the day there are small differences between urban and suburban areas, in fact in urban areas there are often more shadows due to the presence of (usually) tall buildings
- at sunset the thermal inertia of the city is higher then elsewhere, so there the temperature decreases much less then in rural areas leading to the maximum temperature difference during the night

The main contribution to the formation of UHI is therefore the missing night-cooling of horizontal surfaces, together with cloudless sky and light winds. Of course there is also a contribution from indoor heating (during winter), vehicles presence, waste heat from air conditioning and refrigeration systems (anthropogenic effects) but it has been found that they have a minor impact (Taha, 1997).

The usual profile of temperature in the cities is represented in Fig. 1 and the difference between the peak value and the background rural temperature defines the "UHI intensity". The balance among the different components of water fluxes as a function of different landscapes is represented in Fig. 2.

The reduced evapotranspiration observed in a urban landscape (with respect to a rural one) contributes to reduce the cooling of the surrounding air (and increases the fragility of the area in case of floods, but this is another story...). For a more comprehensive analysis of the UHI it is possible to read (among many others) the EPA report (2008) or Shahmohamadi et al., 2011.

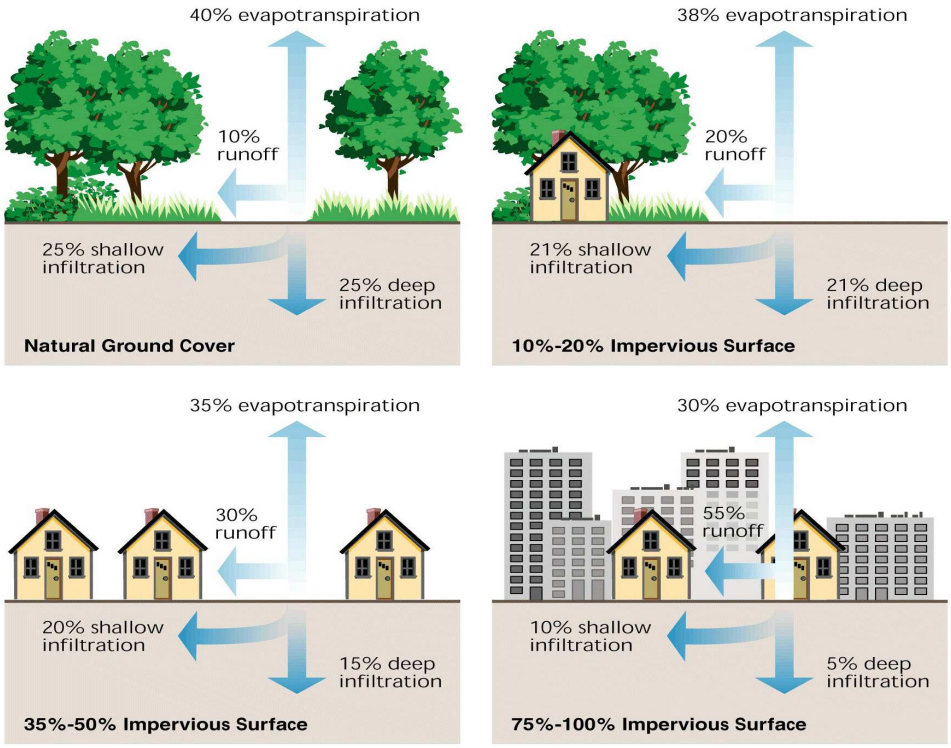

Figure 2: The urban watershed problem (source: the Federal Interagency Stream Restoration Working Group)

2 Methodology

The analysis has been carried out for the years 2009-2010, using data from the ARPA Piemonte ground network (see Fig. 3 for T2m and Rh2m). Since the extension of the UHI is not known, different stations have been considered, some of them far enough from the city center to be considered safely in the rural area.

Values of T2m and Rh2m have been taken and compared during the different months of the year in order to build an average diurnal cycle. All the stations are more or less at the same height (about 250 m asl) for sake of uniformity. This is the reason why the data of Pino Torinese (about 600 m asl) has not been taken into consideration.

Moreover the vertical temperature profiles have been checked using the data of two radiometers (R_1 and R_3 in Fig. 3 above).

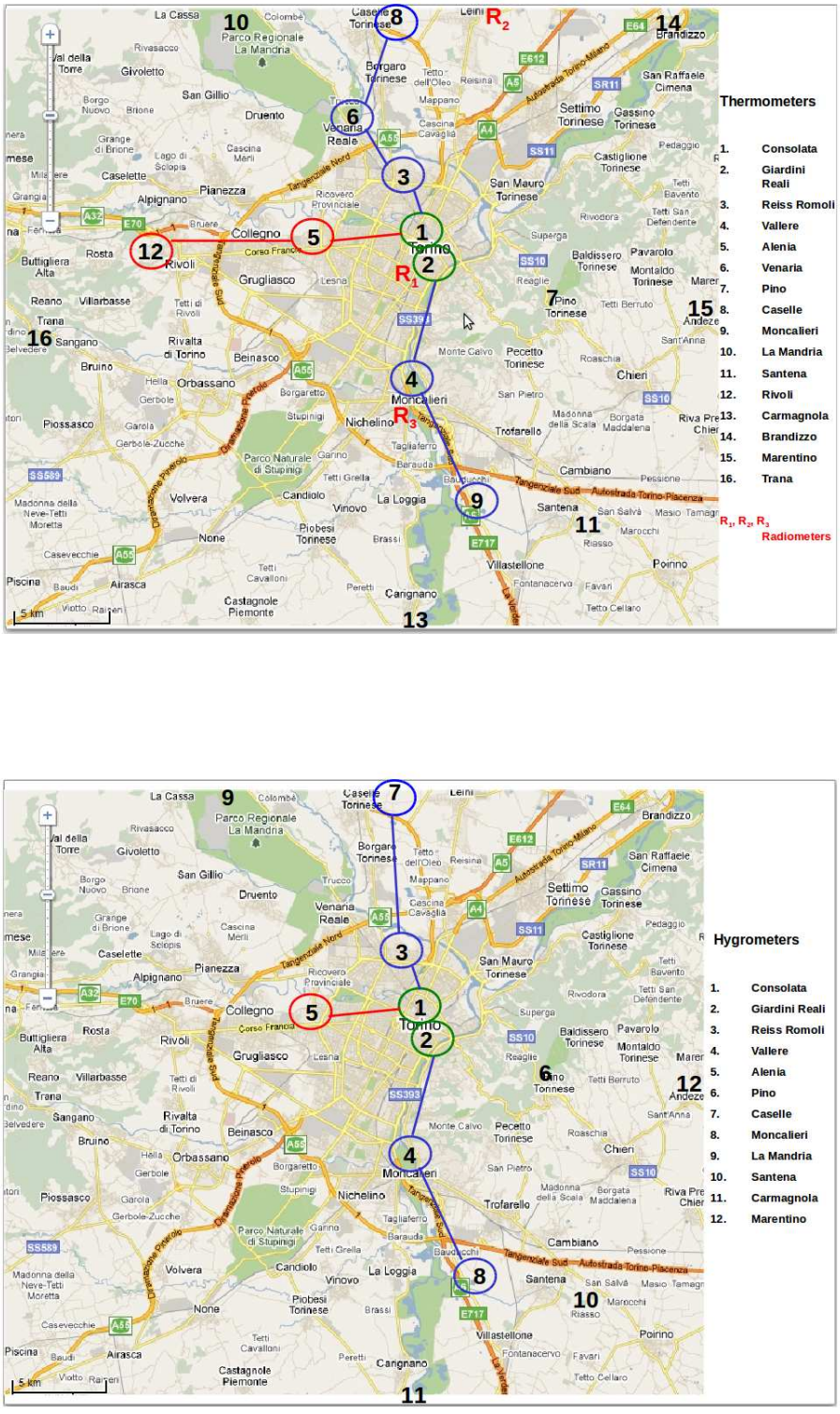

Figure 3: Distribution of the considered thermometers (above) and hygrometers (below) in the Torino area.

3 Results

The results (averaged over 2009 and 2010) are shown according to the two main axis of the city, W-E and N-S, considering the following stations (the correspondence between station number and name is on Fig. 3):

×	W-E	N-S
T2m	12-5-1-2	8-6-3-1-2-4-9
Rh2m	5-1-2	7-3-1-2-4-8

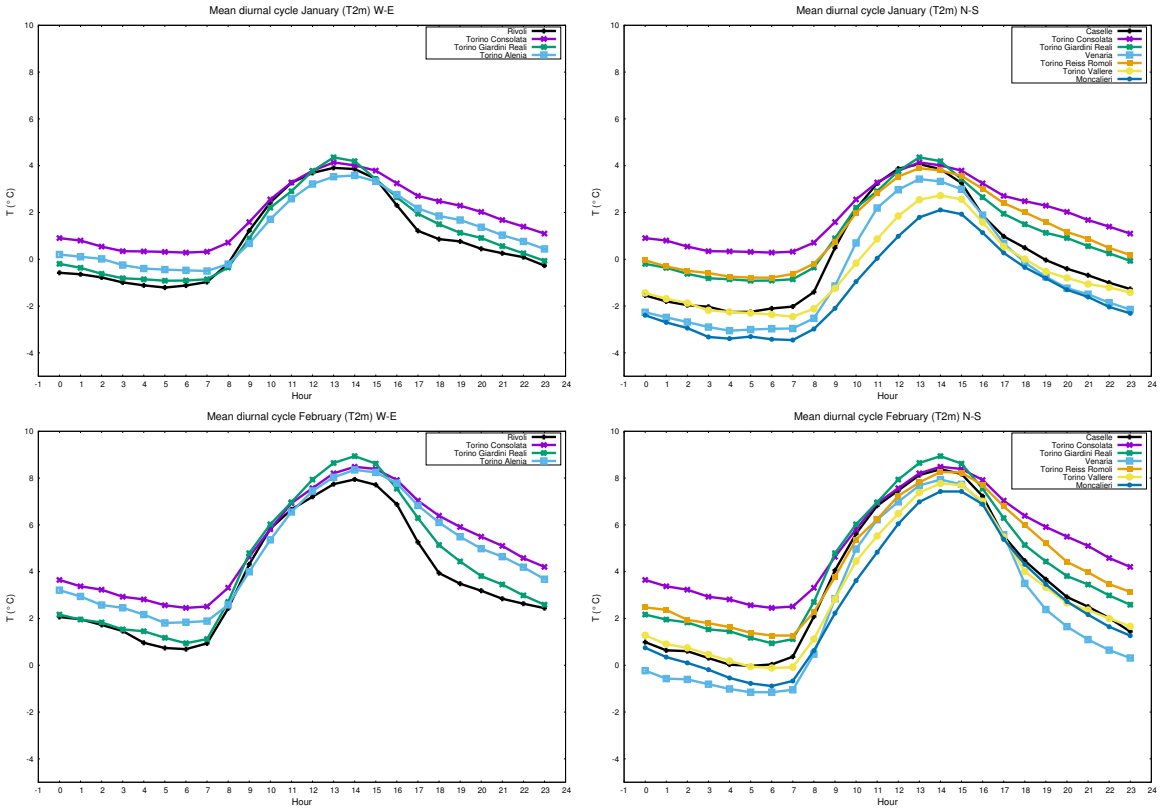

Figure 4: Mean diurnal cycle of T2m in January (above) and February (below), for W-E and N-S sections (left and right respectively)

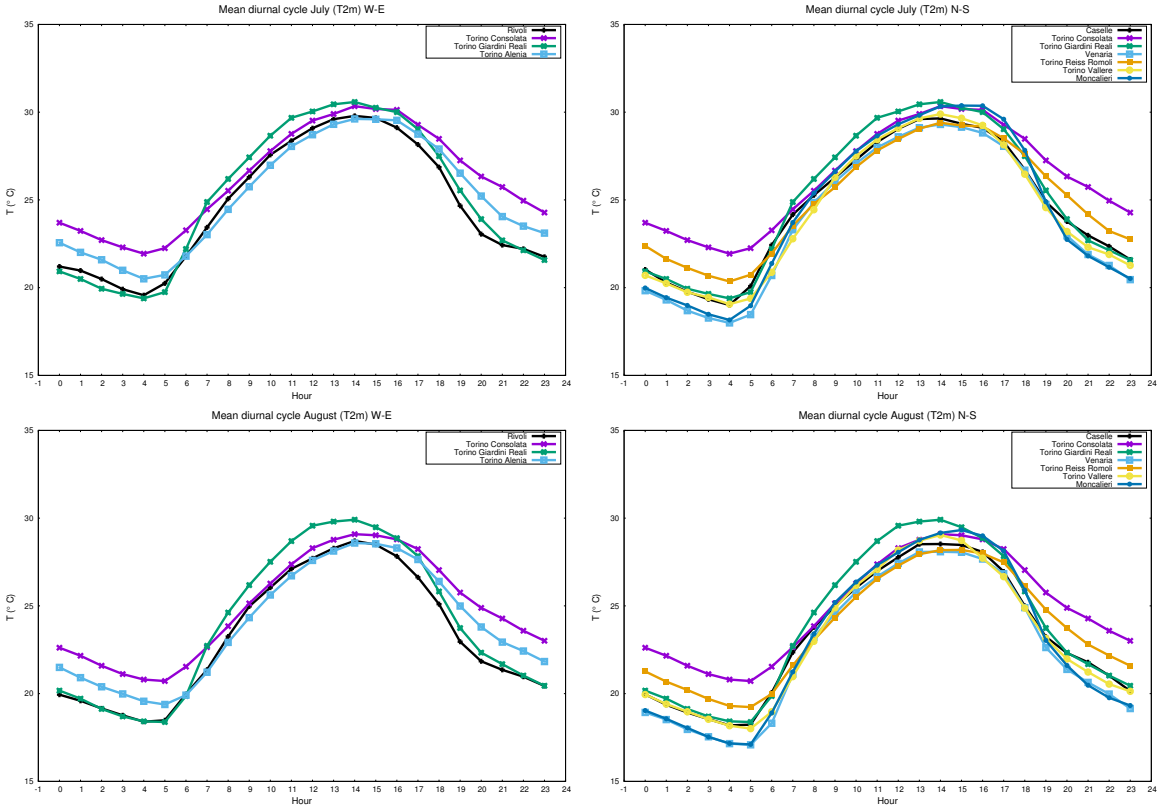

Figure 5: Mean diurnal cycle of T2m in July (above) and August (below), for W-E and N-S sections (left and right respectively).

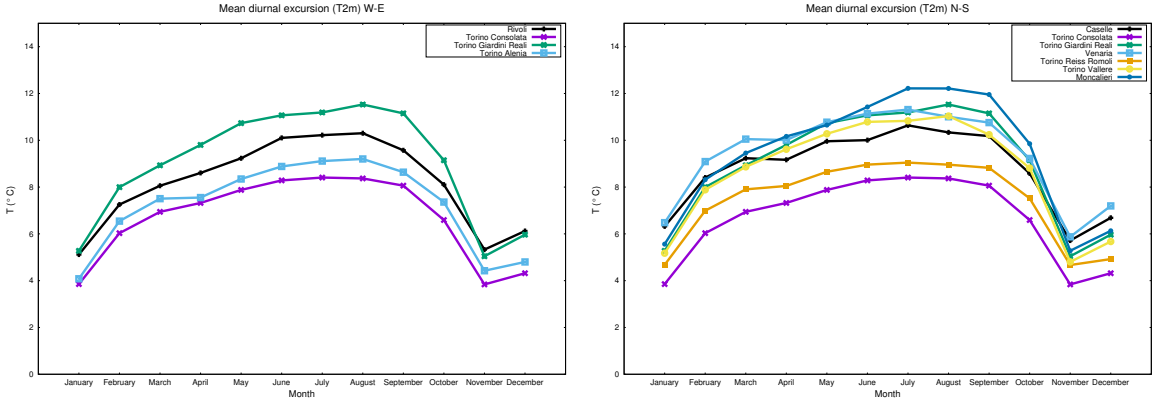

Figure 6: Mean diurnal excursion of T2m as a function of the month, for W-E and N-S sections (left and right respectively).

Looking at the T2m profiles some considerations can be drawn up:

- T2m maxima do not change significantly (the difference ranges from 1 to 2 °C, Figs. 4 and 5) meaning that the incoming solar radiation is the (main) parameter to influence the temperature. There is only the exception of January in Vallere and Moncalieri, but they probably get the morning shadow of the hills that block the insolation, considering that the sun is quite low above the horizon. The effect (which starts in December but it is not shown here) starts to diminish in February and disappears in March (not shown), which seems to confirm the hypothesis
- the differences among the minima is evident and is between 2 and 4 °C, value in agreement with other studies (Bonan, 2001). The reason, as stated before, is that urban areas do not permit the evapotranspiration and the natural nocturnal cooling (Figs. 4 and 5)
- Rh2m variations are quite small during the day and larger during the night but the parameter does not seem to be related to UHI (not shown)

In order to better clarify the presence of the UHI effect, the mean daily excursion (the difference between the mean maxima and the mean minima) has been plotted for each month (Fig. 6). It is evident that the stations of Torino Consolata, Torino Reiss Romoli and Torino Alenia are in the UHI because (especially) during summer the daily excursion is limited, due to the non-sufficient cooling in the night. Torino Giardini Reali deserves a special attention because although it is in the center of the city, it is located in a urban park and therefore it is not correlated to the neighborhood. For the same reason, on the southern side of the city, also Torino Vallere can be considered outside the UHI.

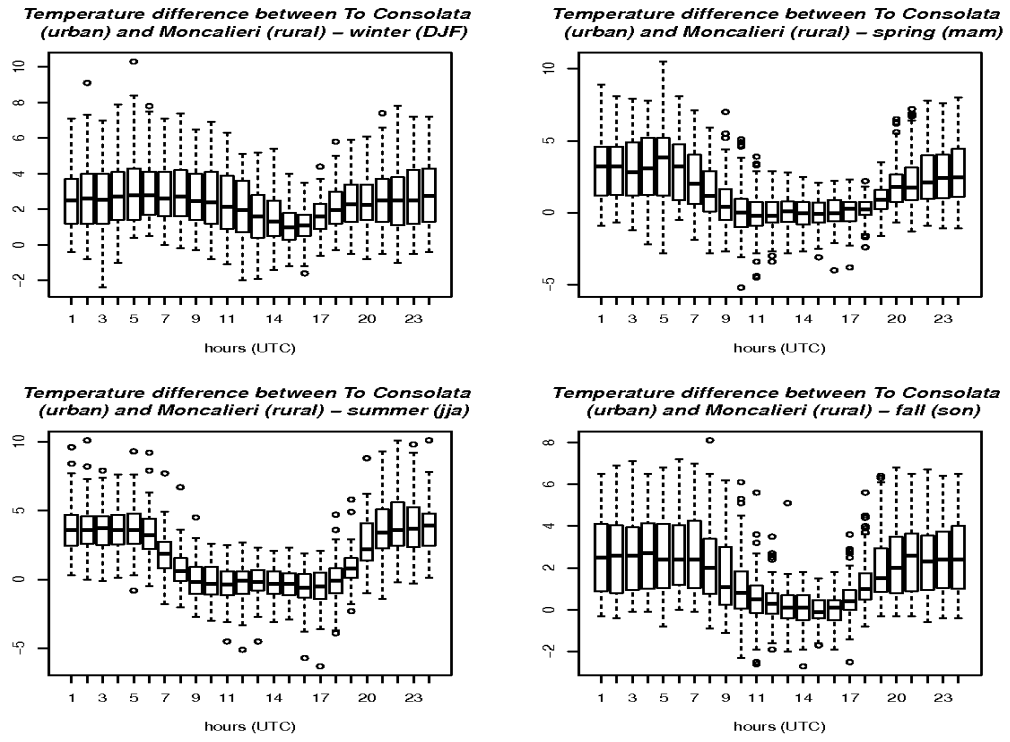

Figure 7: Daily T2m difference between Torino Consolata (urban) and Moncalieri (rural) for different seasons (years 2009-2010).

According to the obtained results, the stations of Torino Consolata (urban, inside UHI) and Moncalieri (rural, outside UHI) have been compared. In Fig. 7 the difference of T2m between the two sites is plotted. It can be seen that the UHI effect is more evident during the night in spring and summer ($\Delta \approx 4$ °C but almost 0 from 9AM to 6PM). During fall the effect is reduced but still present during the night ($\Delta \approx 2$ °C but almost 0 from 10AM to 5PM), while in winter it is more extended all along the day ($\Delta \approx 2$ °C).

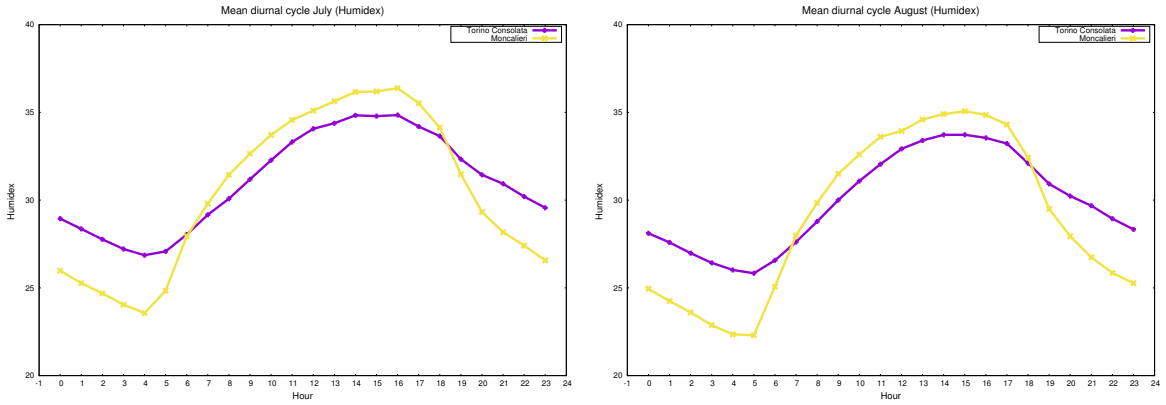

Figure 8: Daily cycle of Humidex index in Torino Consolata (urban) and Moncalieri (rural) in July (left) and August (right) (years 2009-2010).

The same conclusion can be addressed examining Fig. 8 which shows the Humidex index for the same two stations. The Humidex (humidity index) is an index used to describe how hot the weather feels to the average person, by combining the effect of heat and humidity.

It has been developed in Canada (Masterton and Richardson, 1979) and it is a dimensionless quantity based on the dew point according to eq. (1) where T_{air} is the air temperature in ℃ and T_{dew} is the dewpoint in K:

$$H = T_{air} + 0.5555[6.11e^{5417.753(\frac{1}{273.16} - \frac{1}{T_{dew}})} - 10] \quad (1)$$

The adopted convention says that:

- less than 29: no discomfort
- 30 to 39: some discomfort
- 40 to 45: great discomfort; avoid exertion
- above 45: dangerous; heat stroke possible

4 COSMO model evaluation

The same analysis has been performed using the forecast of COSMO-I2 (operational Italian setup). In detail, it has been used the data of 2010 only, 00UTC and 12UTC runs, for the first and the second day (00-24 and 24-48).

Since the data are six-hourly, for sake of comparison, Fig. 9 has been reproduced using only those hours (and only 2010 data of course). The result is shown in Fig. 9.

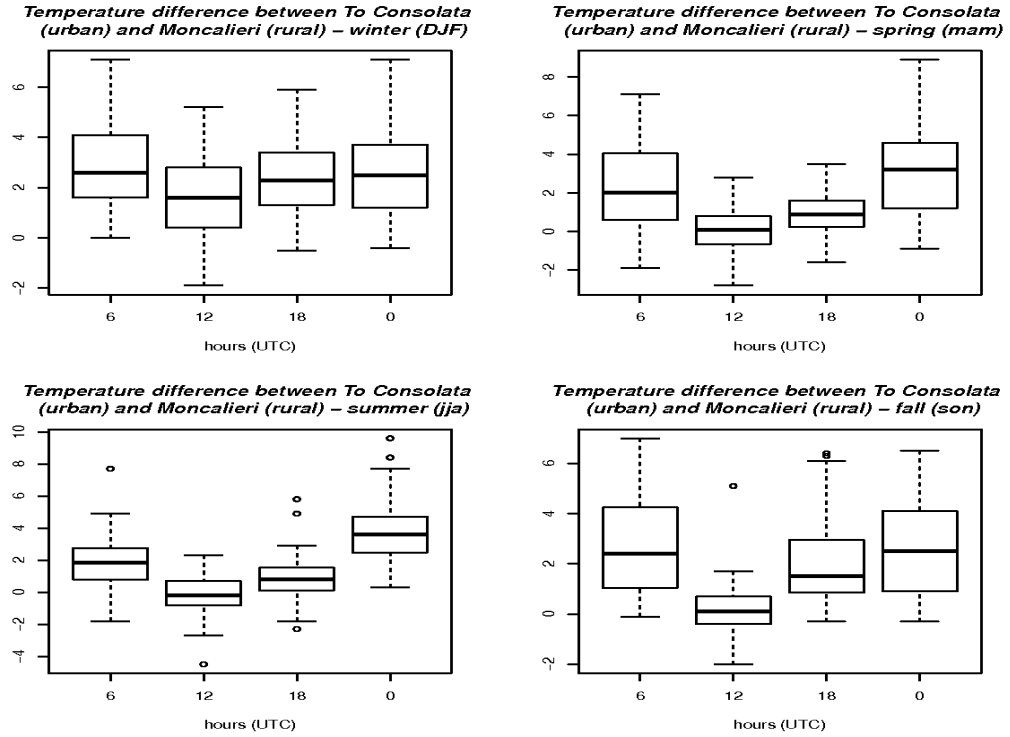

Figure 9: T2m difference between Torino Consolata (urban) and Moncalieri (rural) for different seasons (year 2010), every six hours.

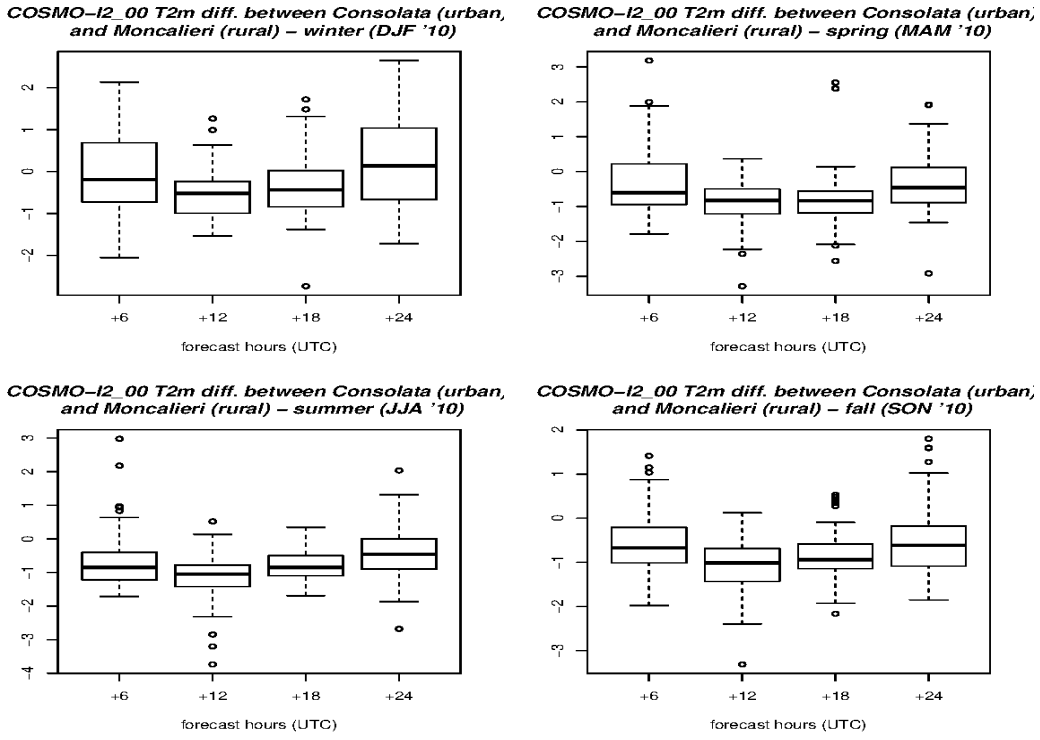

Figure 10: COSMO-I2 (00UTC) T2m difference between Torino Consolata (urban) and Moncalieri (rural) for different seasons (year 2010), from +6 to +24.

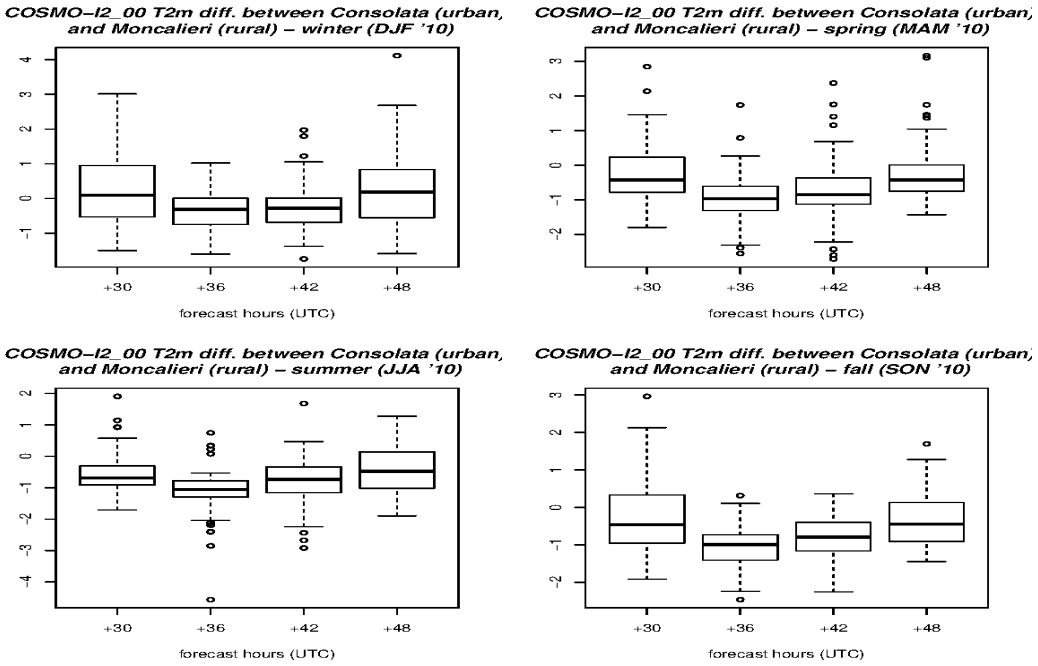

Figure 11: COSMO-I2 (00UTC) T2m difference between Torino Consolata (urban) and Moncalieri (rural) for different seasons (year 2010), from +30 to +48.

It can be pointed out that there is a similar behavior in 00UTC and 12UTC runs (not shown here), in first and second day of forecast, and that there is a considerable difference in the T2m values. In fact in the model the difference amplitude is much less pronounced, that is the two stations (actually the two associated grid points) are too similar and are not able to distinguish the real complexity. This is reflected also in the minor excursion between day and night, which means that the UHI effect is not fully captured, although there is a correct trend in accordance with the observations.

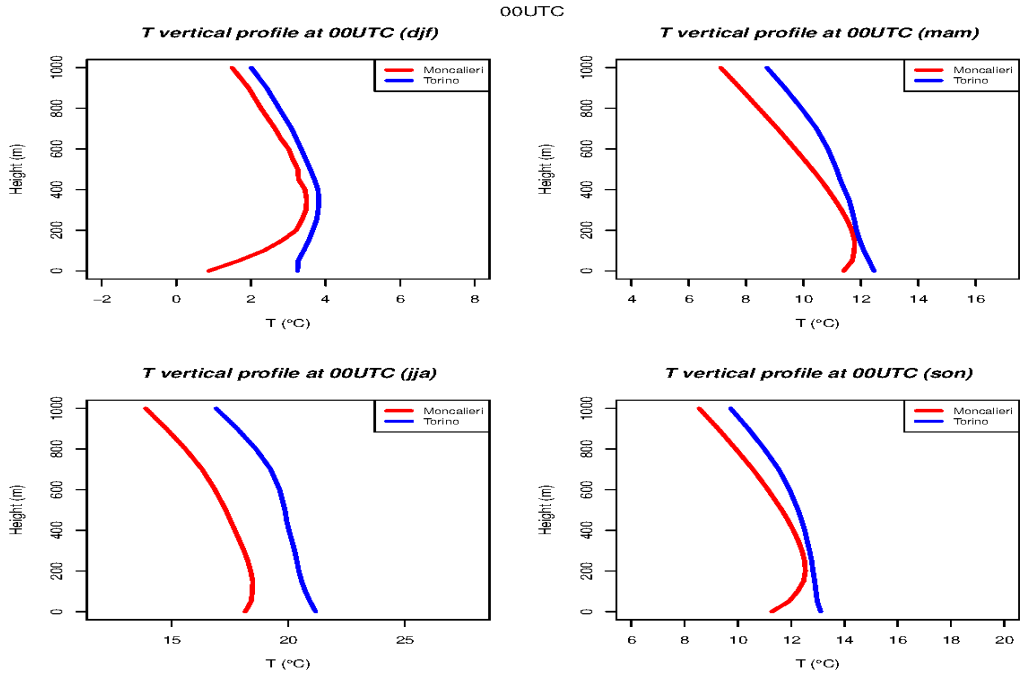

Figure 12: Vertical T2m profile in Torino Consolata (urban) and Moncalieri (rural) for different seasons at 00UTC.

Eventually, the vertical profiles of the radiometers has been examined (see Fig. 3 above). In particular only R_1 and R_3 have been used since they are close to Torino Consolata and Moncalieri respectively. The data have been taken in periods where both radiometers were functioning, that is:

- djf 08/09/12
- mam 08/09
- jja 08/11
- son 08/11

Fig. 12 shows the mean profiles at 00UTC during the different seasons and it is clear that the urban area tends to be warmer than the rural area up to 1000 m. The difference is higher in summer when the nightly boundary layer receives the heat absorbed by the buildings during the day. On the contrary, in winter the difference is concentrated in the lower layers and above 250 m the profiles almost coincide.

5 Conclusions and perspectives

This preliminary work, through the analysis of T2m and Rh2m of different ground stations and two radiometers, clearly highlighted the presence of a UHI effect over Torino. This analysis has to be extended using more recent data. On the other hand it can be seen that the forecast model with a horizontal resolution of about 2 km (COSMO-I2) is not able to represent this peculiar effect. It has to be pointed out that this effect is not parameterized in COSMO (yet) and it probably would need to be studied more in detail. There are examples that go into this direction (for instance Mussetti, 2016), so in the near future it should be possible to test COSMO with this specific parameterization.

References

H. Taha, "Urban climates and heat islands: albedo, evapotranspiration, and anthropogenic heat", Energy and Buildings, vol. 25, no. 2, pp. 99-103, 1997

EPA, "Reducing Urban Heat Islands: Compendium of Strategies", available online at: www.epa.gov/heat-islands/heat-island-compendium, October 2008

P. Shahmohamadi, A. I. Che-Ani, K. N. A. Maulud, N. M. Tawil, and N. A. G. Abdullah, "The Impact of Anthropogenic Heat on Formation of Urban Heat Island and Energy Consumption Balance", Urban Studies Research, vol. 2011, Article ID 497524, 9 pages, 2011

G. Bonan, Ecological Climatology, Cambridge University Press, 2002

J. M. Masterton and F. A. Richardson, "Humidex: A Method of Quantifying Human Discomfort due to Excessive Heat and Humidity", Environment Canada, Atmospheric Environment Service, Ontario, Canada, 1979

G. Mussetti, D. Brunner, S. Henne, J. Allegrini, H. Wouters, S. Schubert and J. Carmeliet, "Impact of model resolution and urban parameterization on urban climate simulation: a case study for Zürich", COSMO/-CLM/ART User Seminar, DWD Headquarter, Offenbach, March 2016

On thunderstorm quantification (continuation)

Jan Parfiniewicz, Jerzy Konarski

Institute of Meteorology and Water Management 61 Podlesna str., PL-01- 673 Warsaw, Poland

1 Introduction

To estimate intensity and create a scale for Extreme Convective Phenomenon (ECP) we are analyzing lightning discharge density field obtained from PERUN lighting detection and location system. PERUN is a polish national weather service's lightning system that provides total lightning information (that is for both cloud (IC) and cloud-to-ground (CG) discharges) over territory of Poland [Parfiniewicz, 2013].

In 2012 a transformation from lightning density field to Virtual Fujita Scale [F] was defined. The transformation was based on correlation between severe weather events reports form SKYWARN POLSKA database and IC and CG data from PERUN SCM total lightning central processor. Two statistical F formulas as a function of lighting densities were invented.

2 Some Formulas and Case Study

The best formula for strong ECP events with number of lightning $[NoL] \geq 1$ under condition that there is at least one CG return stroke and number of cloud signals are more than 70 reads:

1
$$[F_a] = a \times (b \times ICs + c \times ICs)^{1/2} + d$$

where: $a = 0.047$, $b = 0.7$, $c = 0.3$, $d = 0.22$
and IC_s, IC_i are measured in $[NoL/\pi \times 15km^2 \cdot 10min.]$

For less severe events with $0 < [F] \leq 2.5$ another formula that includes CG data (Rs>0) is used:

2
$$[F_b] = a \times (b \times ICs + c \times Rs + d \times (ICs \times Rs)^{1/2})^{1/2}$$

where: $a = 0.088$, $b = 0.624$, $c = 0.112$, $d = 0.264$

Basing on F_a, F_b and taking into account above mentioned restrictions a resulting convective strength F0 is obtained.

In (1,2) IC_s is the first cloud signal registered by PERUN system as starting source emission point. IC_i is a burst of intermediate emission points picturing in two dimension the whole IC event. IC_e is the last emission point signal in given IC event.

The formulae (1,2) indicate that essential data discrimination categories are: IC intermediate data (IC_i), IC starting point data (IC_s) and CG return strokes (RS). Basing on formula studies we can say that IC data seems to play extremely important role in severe weather recognition and development.

The formulae were used to create a nowcast prediction module. It was tested in real time by weather forecasters. There were no heavy thunderstorm or tornado that were missed by transformation formulas (1,2). Overall estimated prediction in 1h forecasts of ECP remains on 90% level.

In 2012 PERUN system was upgraded to newest Vasiala TLP central processor (Vaisala) operating additionally with SCM which remained still operating. As a result two different total lightning datasets were produced by SCM and TLP central processors using the same SAFIR3000's sensor network. From that time 4 new TLS200 locations were added to the network, and 4 SAFIR3000 sensors were changed into TLS200.

We learned that using TLP total lightning data in formulas (1,2) gives different results than SCM data. Despite the fact that CG strokes for TLP and SCM were correlated quite well (about 85%) the most important cloud signals remained practically uncorrelated.

Maximum number of lightning in $[NoL/\pi \times 15km^2 \cdot 10min.]$ TLP vs. SCM								
Is	IC_s	IC_i	IC_e	R_s	S_s	F_a	F_b	F_0
12750.00	6695.00	8513.00	6801.00	1416.00	0.00	3.98	5.99	5.00
1137.00	1314.00	3936.00	1204.00	612.00	295.00	2.16	2.51	2.40
Mean number of lightning in $[NoL/\pi \times 15km^2 \cdot 10min.]$ TLP vs. SCM								
60.64	49.09	30.96	47.82	10.89	0.00	0.44	0.37	0.25
8.28	6.99	13.92	6.97	3.81	1.39	0.29	0.10	0.07
Standard deviation number of lightning in $[NoL/\pi \times 15km^2 \cdot 10min.]$ TLP vs. SCM								
191.29	158.87	127.28	157.86	42.75	0.00	0.22	0.36	0.38
24.70	24.53	60.47	24.36	14.57	7.82	0.12	0.17	0.15
Correlation of individual category from Is to F_0 TLP and SCM with F_0/SCM.								
0.41	0.38	0.21	0.38	0.43	0.00	0.42	0.49	0.52
0.62	0.70	0.46	0.67	0.50	0.33	0.74	0.87	1.00
Correlation of individual category Is to F_0 TLP vs.SCM								
0.42	0.28	0.15	0.30	0.85	0.00	0.36	0.47	0.52

Statistics for comparison of SCM and TLP datasets in categories of IC and CG and formulas – (F_a, F_b, F_0) is expressed by maxima, average, standard deviation, and correlations of relevant lightning discharge discrimination categories with result scale factor F_0, and correlations SCM/TLP for each of IS, $IC_s, IC_i, IC_e, R_s, S_s, F_a, F_b, F_0$,

where:

- Is – Isolated emission points,
- IC_s – Intracloud start points,
- IC_i – cloud intermediate source locations,
- IC_e – cloud end points
- R_s – return strokes,
- S_s – subsequent strokes
- F_a – filter No 1. based on IC_s & IC_i, responsible for extreme tornado events,
- F_b – filter No 2. based mainly on R_s, when responsible for strong convective events with the prospect of weakening,
- F_0 – resulting convective strength.

Statistics were performed for period from 2014.07.29 to 2015.08.10, with total number 5485 studied 10 minutes episodes. Each episode is a density field for a domain over whole Poland (net 113 x 101 with 7 km grid). In total from which 231173 cases (grid points) were selected.

4 Resume

The most probable reason of low correlation of IC events between two systems is lack of sophisticated TLP data calibration (*Lightning Network Performance Evaluation Program-NPEP*) after the network upgrade. End of lightning season caused that the NPEP was not possible. Moreover four Safir 3000 sensors were changed into TLS200 sensors resulting in lowering density of Safir network.

We are planning to repeat the described comparison with recalculated TLP dataset when NPEP is performed at the beginning of 2016 lightning season. Transition from SCM to TLP data for formulae (1,2) is possible because of fact, that TLS200 and Safir3000 sensors are using basically the same signal filtering for IC.

References

[1] Vaisala, 2003+: SAFIR 3000–3, User Manual, DS Settings and Control Manual, Release 2.3, Helsinki, Finland, **July 2003**.

[2] http://www.vaisala.com/en/products/thunderstormandlightningdetectionsystems/Pages/TLS200.aspx

[3] http://www.vaisala.com/en/products/thunderstormandlightningdetectionsystems/Pages/tlp.aspx

[4] Parfiniewicz J., 2012: Concerning Thunderstorm Potential prediction. The European Meteorological Society Annual Meeting and 9^{th} European Conference on Applied Climatology, *d*, Poland,10-15 September 2012. Abstracts vol.9, EMS2012–81.

[5] $http://meetingorganizer.copernicus.org/EMS2012/EMS2012-81.pdf$

[6] $http://presentations.copernicus.org/EMS2012-81\_presentation.ppt$

[7] Parfiniewicz J.,2013, On thunderstorm quantification, COSMO Newsletter No. 13;
$http://www.cosmo-model.org/content/model/documentation/newsLetters/newsLetter13/cnl13\_07.pdf$

[8] Parfiniewicz J., 2013. Nowcasting strong convective events (SCE) – the Thunderstorm Thermometer, Meteorological Technology World Expo 2013, Brussels, Belgium, 15 -17 oct.$http://www.ukintpress-conferences.com/uploads/SPMTWX13/Breakout\_Session\_d2\_s2\_p5\_Jan\_Parfiniewicz.pdf$

[9] Parfiniewicz J., 2014: Steps to a storm forecasting and nowcasting strong convective events, Meteorological Technology International, **48**;
$http://viewer.zmags.com/publication/c4f984ab\#/$c4f984ab/50.

[10] Parfiniewicz J., 2014. Between forecasting and nowcasting strong convective events. COSMO newsletter no.14 http://www.cosmo-model.org/content/model/documentation/newsLetters/newsLetter14/default.htm

[11] Parfiniewicz J., Barański P., 2014. An Explosive Convection over Europe with 8-Minute Tornado Incident in Poland on July 20, 2007. Int. J. Environ. Eng. Nat. Resour. Volume 1, Number 6, 2014, Łazarewicz W., Parfiniewicz J., Walasek J., 2012-2016 http://awiacja.imgw.pl/index.php?product=burze **262-276**

[12] Łazarewicz W.,Parfiniewicz J.,Walasek J.,2012-2016,$http://awiacja.imgw.pl/index.php?product=burze$.

Assessment of model generated wind energy potential in Poland.

Katarzyna Starosta, Andrzej Wyszogrodzki

Institute of Meteorology and Water Management – National Research Institute. PL-01-673 Warsaw, 61 Podleśna str.; katarzyna.starosta@imgw.pl; andrzej.wyszogrodzki@imgw.pl

Summary

The aim of this paper is to show the suitability of using numerical model wind speed forecasts for the wind power industry applications in Poland. Based on the six months January-June climatology of wind speed data, potential energy zones within the area of Poland have been assessed. For the practical interpretation and further post-processing, results of the numerical model COSMO at 2.8km resolution were verified against data from 60 SYNOP stations.

The verification is performed by comparison of wind rose plots from model simulations and observations at individual station locations. The good agreement is observed over the most homogeneous zone with highly preferred wind speed for the wind energy potential. The smaller agreement is observed at the coastal stations and in the large urban agglomerations.

1 Introduction

In accordance with the guidelines of the European Union, the use of Renewable Energy Sources (RES) increased significantly in the last few years. This embraces tendency of the energy production in a close proximity to the end customers. Thus in addition to large wind farms many small installations have been created in residential areas, farmlands and small businesses. RES technologies have currently high overhead due to investment costs, which translates to a long financial recovery period. Therefore, an appropriate selection of location and even the characteristics of the source of energy is an important issue. At the end of 2015 year, up to 2/3 of RES installations in Poland were based on the wind energy [1].

Estimation of the wind energy potential for the selected location is a key factor and at the same time one of the most difficult steps in making decision in the process of implementation of RES installations. More over the natural processes of climate change and scattered growth of urban zones where consumption of energy is the highest contributes to the increased uncertainty in the development of RES industry.

Since the wind energy is natural weather element highly variable in time and space, it requires detailed studies using different approaches. The climatology of wind speed data is the first criterion for assessing the location of the wind farm. However the typical station network routinely used for this purpose is vastly sparse and does not allow for reliable estimation of spatial and temporal variability of renewable energy resources, especially in the areas affected by the topography or in the close proximity to urban locations.

On the other hand the meteorological models are helpful in estimating the energy resources in the locations where there is lack of measurements or when sensor network does not provide complete data. Currently running operational numerical weather prediction (NWP) models increases their spatial resolution allowing for more adequate representation of the meteorological conditions, even those prevailing within the urban area. Application of numerical model allows for a more detailed study on the role of the individual processes such as radiation properties and wind flow structure, affecting the local climate diversity. Before use of gridded data for estimate the potential energy zones, numerical weather model analysis and forecasts must be verified against the measurements at the available network stations.

2 SYNOP stations and COSMO model configuration.

Currently, RES in Poland are calculated either by the local climatology or as the result of interpolation of current measurements from nearby weather stations.

The annual distribution of the wind energy potential on Figure 1 (i.e. the map "Zones of wind energy in Poland" from [2] Lorenc 1996) based on wind speed data collected between 1976-2005 provide the basic information for investors in the first stage of the selection of wind farms location.

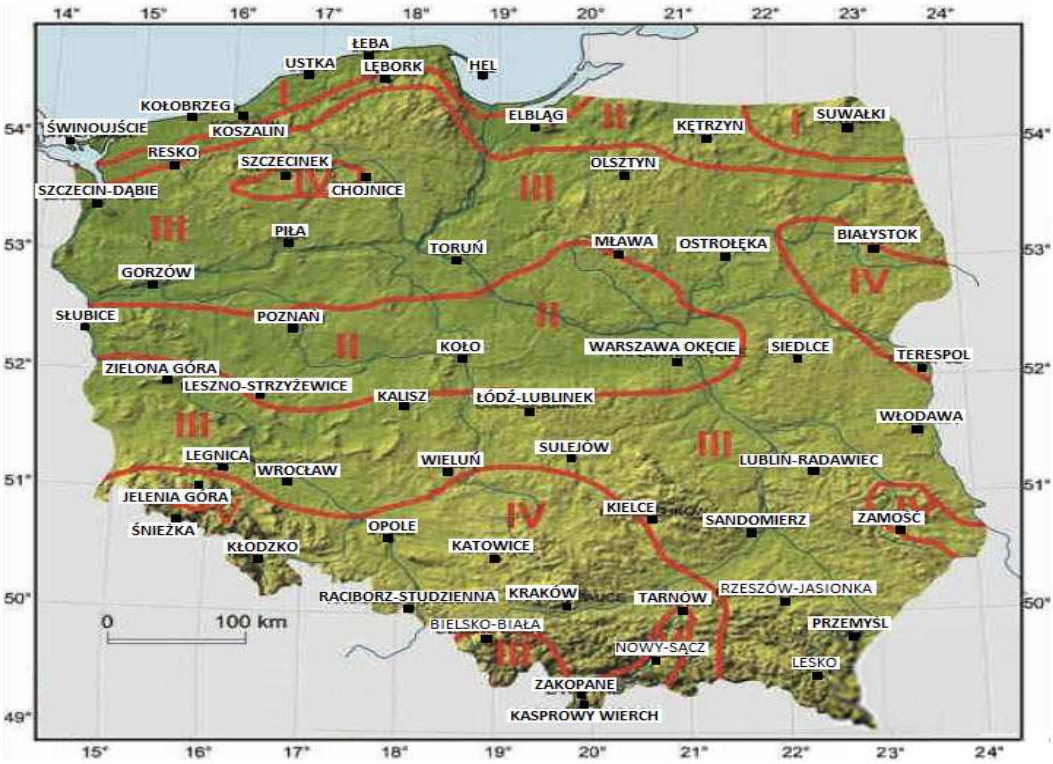

Figure 1: Zones of wind energy in Poland from Lorenc 1996.

Zone	Name of zones	Numbers of synop stations
I	extremely favourable	6
II	very favourable	10
II	favourable	21
IV	less favourable	9
V	unfavourable	3

The Polish Institute Meteorology and Water Management – National Research Institute (IMWM-NRI) runs an operational model COSMO (Consortium for Small-scale Modelling) employing two nested domains at horizontal resolutions of 7 km and 2.8 km (as seen on Figure 2) with 78 hour and 36 hour forecast respectively.

Both models runs four times per day starting at 00, 06, 12, 18 UTC. The COSMO model forecast require provision of the initial state (IC) and boundary conditions (BC) for the whole simulation. The input data are obtained from global ICON model working on icosahedral-hexagonal grid, which runs operationally four times per day at Deutscher Wetterdienst (DWD). The highest spatial resolution of ICON model over Europe equal to 13 km with the forecast time span of at least 78 hours.

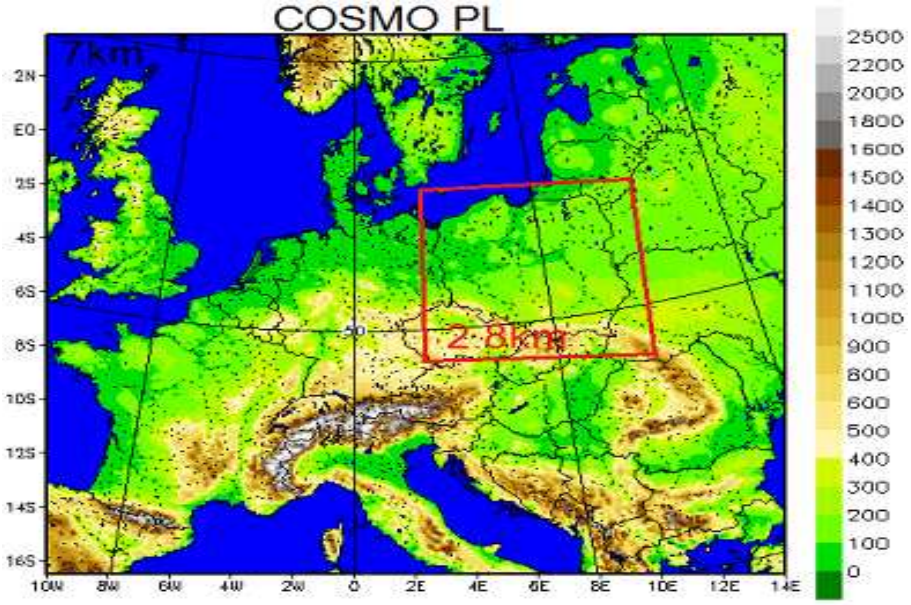

Figure 2: COSMO model domains at 7.0 km and 2.8 km horizontal resolution.

Implemented in COSMO model observational data assimilation (DA) system is based on the nudging technique and allows for ingesting weather data measurements - as e.g. these carried out on SYNOP stations - to improve forecast's quality. Data used in the assimilation cycle of the operational COSMO model at IMWM-NRI are acquired from the WMO/GTS network by the SkyGlobus system.

3 Case study results

In order to make a fair assessment of the reliability of results obtained with the COSMO model, it is necessary to verify model forecasts with available measurements.

In the current section, the 24 hour COSMO 2.8km model forecasts (starting at 00UTC) were compared with continuous observations carried out at 60 SYNOP stations collected in the first half of the 2014 year between January and June. The station locations and their description is presented at Figure 1.

Region/ city stations	Calm %		Average m/s		Resultant vector deg/%		Dominant direction		Dominant class speed m/s	
	synop	model	synop	model	synop	model	synop	model	synop	model
Zone I 6	0.73	0.42	3.93	4.79	161/16	170/19	S,W,E	S	0.5_2.1	3.6_5.7
Zone II 10	3.31	0.51	3.73	3.73	130/9	161/13	E,W	SE,W,E	3.6_5.7	3.6_5.7
Warszaw	11.14	0.48	3.37	2.90	60/10	141/8	W,SEE	SE	0.5_2.1	0.5_2.1
Zone III 21	2.95	0.60	3.22	3.55	148/6	174/10	W,E	W,SE	0.5_2.1	0.5_2.1
Zone IV 9	5.03	1.17	2.89	3.37	232/1	166/5	S, W, E	S,W	0.5_2.1	0.5_2.1

Table 1: The characteristics of the wind in the individual zones

Table 1 contains the wind characteristic of SYNOP data and model forecast in the diverse energy zones from Figure 1 and at the urban location within the city of Warsaw. The best agreement in terms of average wind speed and wind direction is seen in Zone II, the lesser agreement is observed in the Zone IV and at the urban

location in Warszawa. In order to better interpret the above statistics we have computed additional results in the form of wind roses generated from NWP model and SYNOP stations, averaged within each zone. A wind rose is a concise and illustrative product analyzing wind speed and wind direction at a certain location. It provides information about the frequency of winds at certain speed ranges and particular direction, as well as its time percentage. In current calculations the WRPLOT View program was utilized to generate appropriate plots [3].

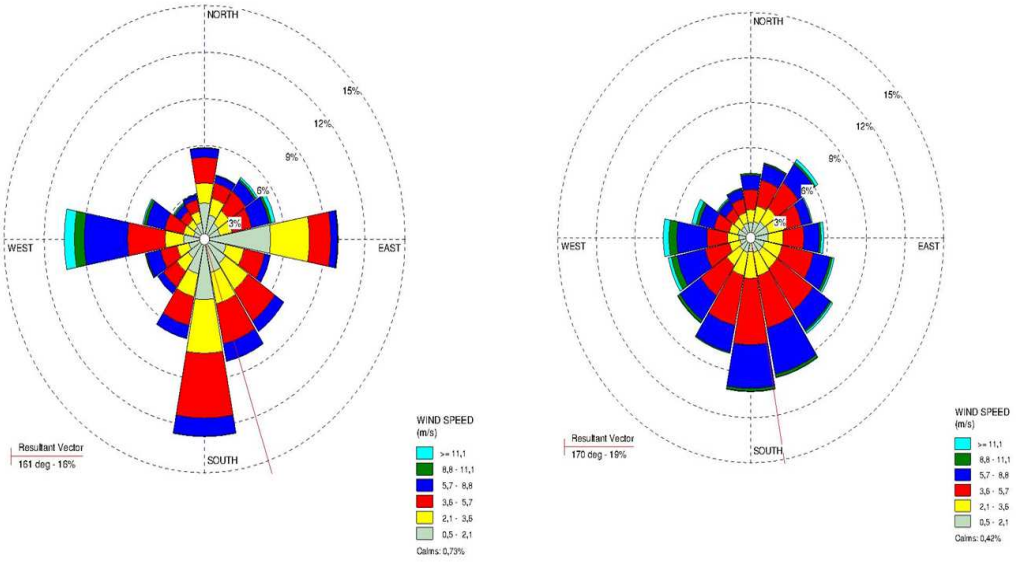

Figure 3: Wind roses for Zone I (6 stations) averaged between January-June 2014: SYNOP stations (left), COSMO model (right)

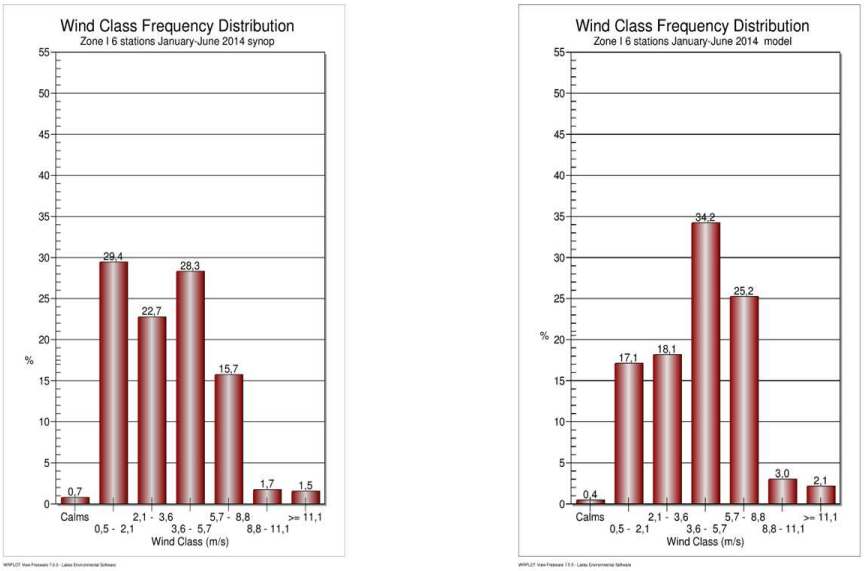

Figure 4: As in Figure 3 but wind class frequency distribution

Zone I (extremely favorable), covers the seaside area in Poland and north-eastern corner of the country. In the analyzed period, 65% of the forecasted winds were very favorable for the production of energy. In this zone, the wind directions are very diverse. The average wind speed predicted in the model is significantly higher than the observed one. The maximum wind speed of synoptic data from the selected wind directions are higher than data from the model. This situation is associated with the coastal station locations, and requires

more detailed research for each location.

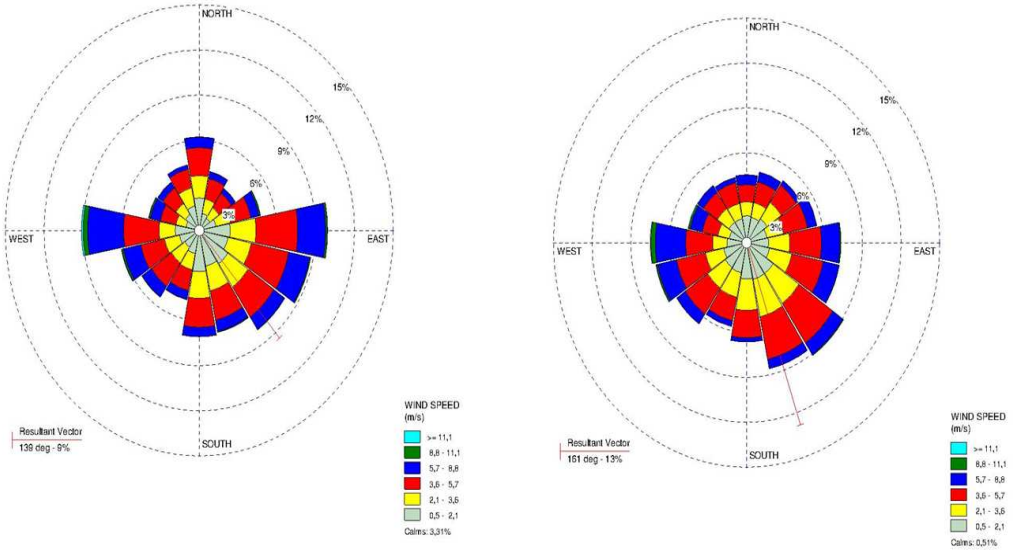

Figure 5: Wind roses for Zone II (10 stations) averaged between January-June 2014: SYNOP stations (left), COSMO model (right)

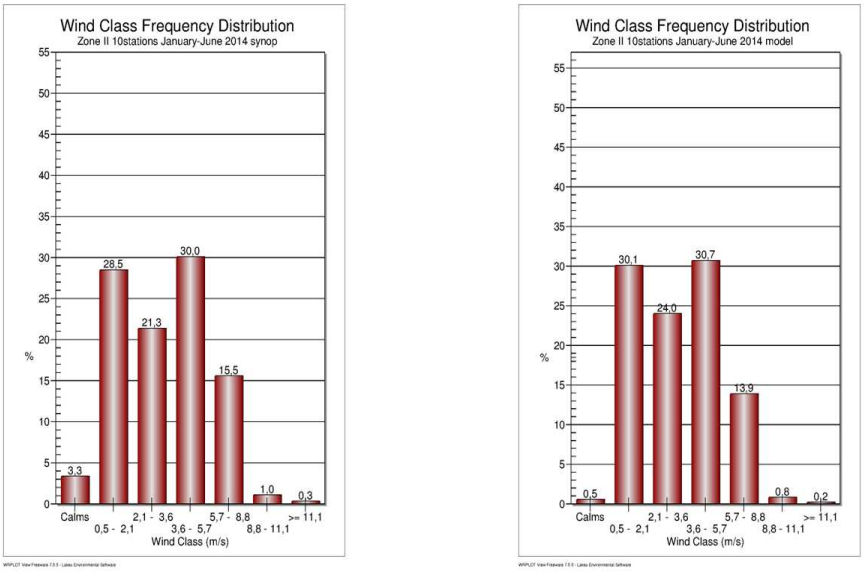

Figure 6: As in Figure 5 but but wind class frequency distribution.

Zone II (very favorable area) - is the most homogeneous with highly preferred situation of wind speed. It covers a continuous area of the central Polish lowlands and is the only zone where the dominant is the class of wind speed range 3.6-5.7 m/s for both prediction and observation. In this zone, the average value of wind speed predicted from COSMO model is the same as from observations. The consistency is also observed analyzing frequency distribution of particular wind speed classes.

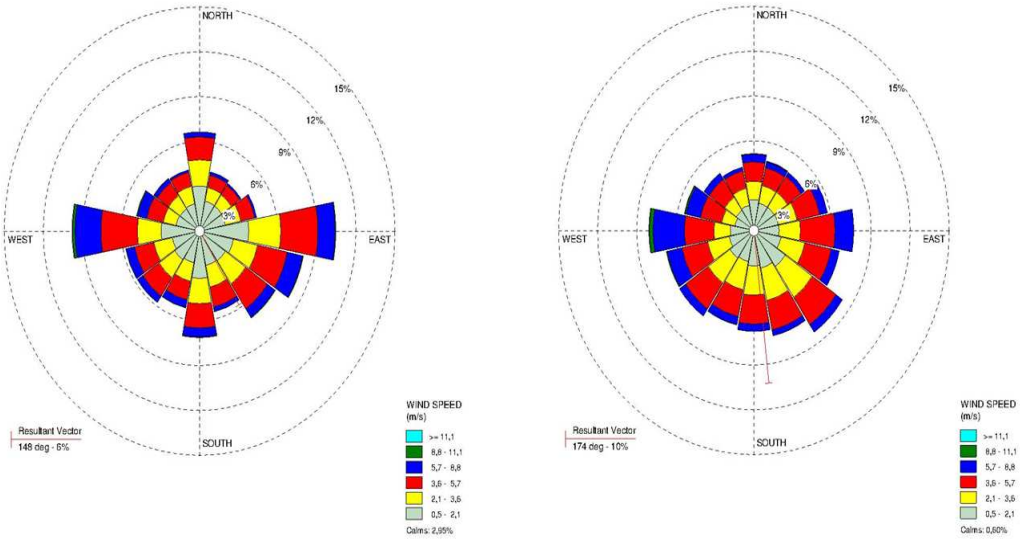

Figure 7: Wind roses for Zone III (21 stations) averaged between January-June 2014: SYNOP stations (left), COSMO model (right)

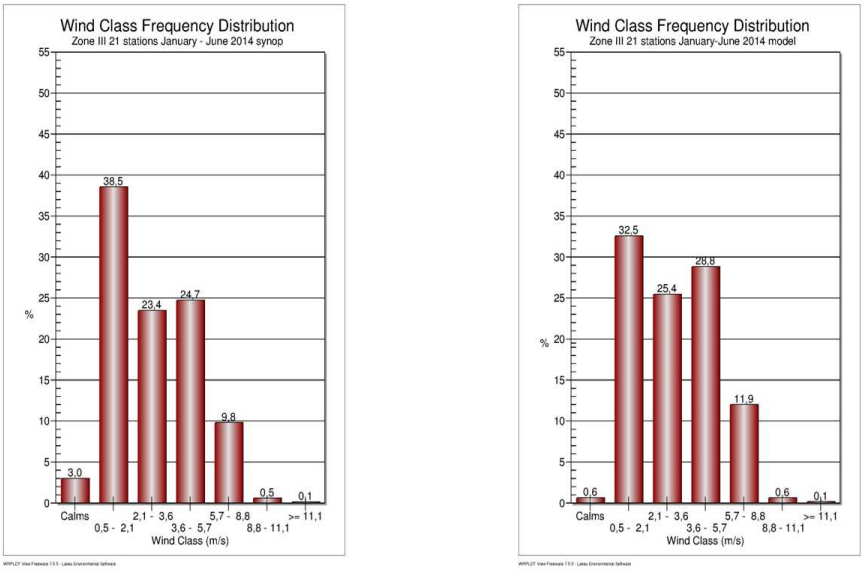

Figure 8: As in Figure 7 but wind class frequency distribution

Zone III (favorable) covers the largest and very diverse area, including lake districts, upland areas and the low mountains. We are observing in this zone a slightly higher wind speed forecasts than the observed average wind speed. The maximum values for wind speed are higher for the observations. In this zone, the lowest class of the observed wind speed show higher frequency of the distribution then the model forecast one.

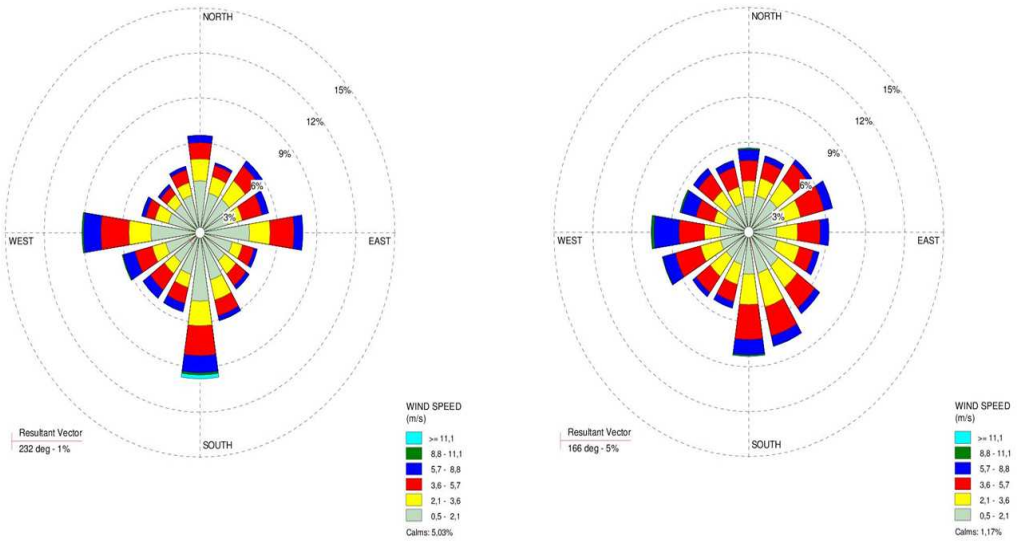

Figure 9: Wind roses for Zone IV (9 stations) averaged between January-June 2014: SYNOP stations (left), COSMO model (right)

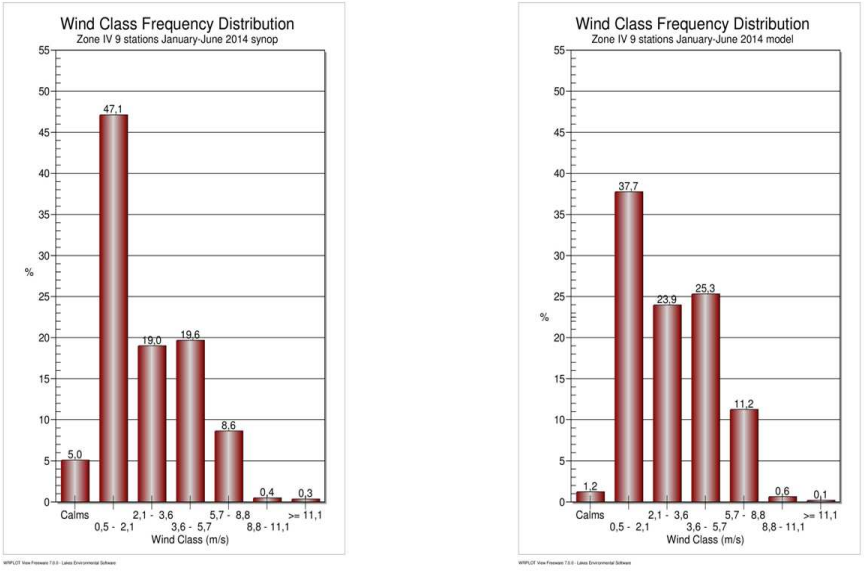

Figure 10: As in Figure 9 but wind class frequency distribution

Zone IV (less favorable) includes foothill and mountain areas with highlands and plateaus in the eastern part of the country. Due to the nature of the zone observed wind directions are varied. In this zone there is also a significant amount of (5%) calms with little or no air movement. A bit higher speeds are predicted in the model than observed at the stations.

The zone V Including mountainous terrain is unfavorable for wind energy, and has been omitted from the current analysis.

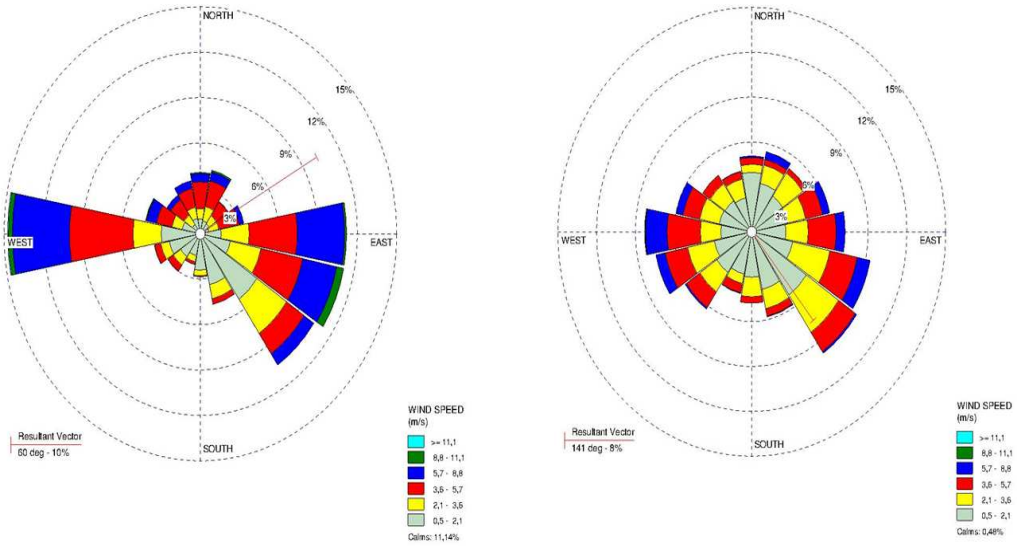

Figure 11: Wind roses for Warszawa averaged between January-June 2014: SYNOP stations (left), COSMO model (right)

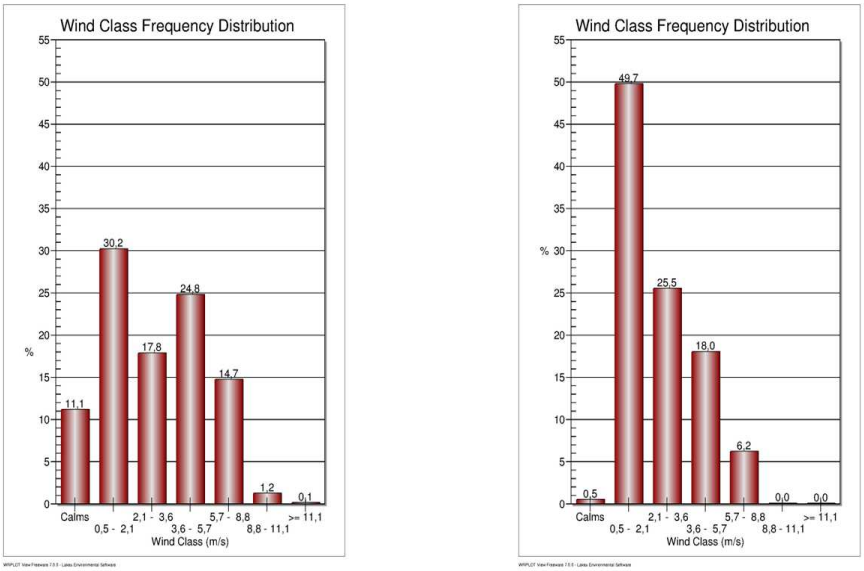

Figure 12: As in Figure 11 but wind class frequency distribution

Synoptic station in Warszawa is located in the south-western part of the city, at the Okęcie airport. A big urban agglomeration as Warszawa shows higher errors than the average error for the same zone. At the weather station there is observed significant amount of calms (11%). In the model, this translates into a very large percentage of small-wind speed (50%).

4 Summary and Outlook

Our motivation to perform presented here analysis of the COSMO model wind forecast as the source of energy potential in the area of Poland was the increased interest in renewable energy applications, which is associated with recent EU guidelines. An increasing awareness about the benefits of clean energy, results in the intensified development of traditional wind farms, as well as in micro installations and smart grids. The presented wind rose analysis depicts in each of the wind zones the frequency occurrence of particular classes of wind speed and wind direction for a given location and time period. In the comparison with synoptic measurements we observe larger number of listed periods of silence, which in the model is generally at the level below 1%. The interpolation of model gridded data into the point station locations enhances this effect by allowing greater spread of the wind directions and generally reduced maximum speed of the wind. The largest forecast errors are observed in the Zone I and are associated with the coastal effects at the interface between land and sea. Whereas in other zones forecast errors are much smaller. In the zone III, we observe the underestimation of the lower wind speeds by the model and overestimation of the greater wind speed amplitudes. Large urban agglomerations as Warszawa produces significantly higher errors than the average errors in the same zone. The complex structure of the urban areas is currently a challenge for the generation of representative urban meteorology and will be the subject of further investigations.

References

[1] Energy Regulatory Office - http://www.ure.gov.pl/ (in polish)

[2] Lorenc H., 1996, Struktura i zasoby energetyczne wiatru w Polsce, Materiały Badawcze, Seria: Meteorologia -25, IMGW, Warszawa (in polish).

[3] Lakes environmental software _WRPLOT View - *http : //www.weblakes.com/products/wrplot/*

Verification of results of the working technology SNOWE for snow water equivalent and snow density fields determination as initial data for COSMO model

E. Kazakova, I. Rozinkina, M. Chumakov

1 Introduction

Atmospheric models need snow water equivalent (SWE) and snow density values as initial fields. However, currently no operational SWE measurements are carried out with the spatial and temporal resolution needed for mesoscale models. Only seasonal specific observations are conducted in 5-10 days interval SYNOP measurements of snow depth is the only regular operational information describing snow cover characteristics, since satellite data contain information only on the position of snow cover boundary. Snow density calculation is based on 'age functions', which describes snow evolution quite robust. SWE is obtained from these snow density values and measurements of snow depth. The snow density values depend on thermal history of the entire cold period of the year.

These values could be obtained using empirical relationships, which allow converting snow depth into needed density values, which results of SWE simulation during continuous data assimilation system (DAS) cycles resulting in turn in accumulation of errors. According to the previous research [Kazakova, Rozinkina, 2011], COSMO-Ru model simulates SWE with discrepancies (relative errors of the model versus measured SWE values could be as high as $200 - 300\%$. RMS errors were about 10 mm at the southern European part of Russia and up to 130 mm in the North) independently of snow parameterization used in the model. This results in wrong calculation of heat budget components near snow edge and wrong T2m forecasts in this narrow frontier zone.

2 Goals

For NWP purposes there is a need to use only station observations as the most reliable source of information on snow cover. Therefore it is required to develop such an algorithm which could allow to calculate snow cover characteristics using only the data of standard meteorological observations (in SYNOP code) transmitted every 3 hours. Such algorithm should consider the main processes in snow cover during its existing period, which could be described only using station observations without excessive details, which could significantly increase the computational time of snow characteristics assessment. A snow model satisfying these requirements is presented in further sections. Based on this snow model, the technology of SWE and snow density initial fields generation was developed. The results of its processing in quasi-operational regime in winter 2014/2015 are discussed.

3 Brief description of the snow model SMFE

Developed one-dimensional multi-layer parametric snow model SMFE (Snow Model Finite Element) is based on standard meteorological observations – snow depth, air temperature, dew point temperature, wind speed, 12-hour accumulated precipitation [Kazakova, Chumakov, Rozinkina, 2013].The realized SMFE model is based on the main principle that snow column is represented as a number of layers (hereinafter referred as elements) which are in thermal and mechanical interaction with each other. The height of an element h in the given realization is set to 1 cm in accordance with the accuracy of this characteristic within the framework of SYNOP-code. Consequently, the number of elements is counted according the measured snow depth (cm) at each station. Since in time $t_0, t_1, \ldots, t_k$ (during 'snow' season) snow depth at station changes, the number of elements will also change.Brief description of the algorithm principle is presented on the scheme (Fig.1).

The model starts operating as soon as the measured snow depth differs from zero. At each time step (1 day) the amount of new elements in dependence on snow depth variations $\triangle H$ is defined: $N_{t_k} = N_{(t_{k-1})} + \triangle N$ where $\triangle N = \triangle H/h$.

If $\triangle N > 0$ (case of snow falling, then density of the newly fallen upper layers (fresh snow with depth $\triangle H$),is calculated in dependence on daily-averaged air temperature according to empirical equation 1 [Bartlett, MacKay, Verseghy, 2006]:

$\rho_{s,f} = 67.92 + 52.25^{\frac{T_a}{2.59}}, T_a \leqslant 0^oC$; $\rho_{s,f} = min(200; 119.2 + 20T_a), T_a > 0^oC$;

where $\rho_{s,f}$ - fresh snow density,kg/m^3,

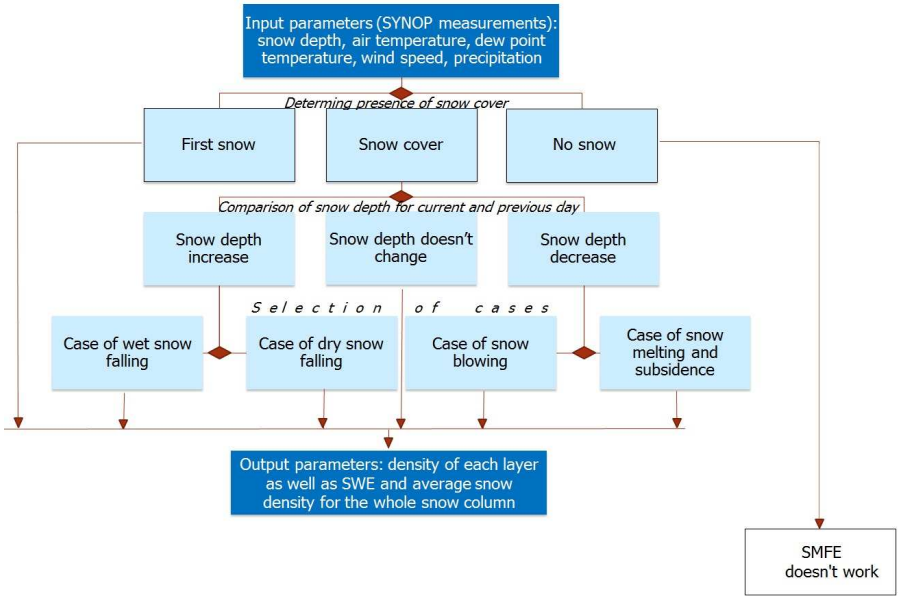

Figure 1: The schematic diagramme of the model SMFE. Dark blue rectangles represent the input and output parameters.

For 'lying' snow (not considering new 'fresh snow' layers) variation of element density at each time step $\triangle\rho_n(t_k) = \rho_n(t_{k-1}) + \triangle\rho$, (where $n(t_k) = 1, \ldots, N(t_k)$ is a serial number of an element),is determined, when $\triangle N \neq 0$. Component $\triangle\rho$ contains information about increase/decrease of an element density in dependence on the value of $\triangle N$:

$\triangle\rho = \rho + \rho + \rho$

where ρ - case of snow compaction on account of new elements($\triangle N > 0$), ρ - case of snow compaction due to snow blowing ($\triangle N < 0$), ρ - case of snow compaction dew to subsidence or melting (percolation of water and its freezing)($\triangle N < 0$). If $\triangle N > 0$, the density of each element

$$\rho_n(t_k = \rho_n(t_k))T_n(t_{k\smile}), \sum_{m=n(t_k)}^{N(t_k)} \rho_m(t_k) \tag{1}$$

would be a function, depending on air temperature $T_n(t_{k\smile})$ at time $(t_{k\smile})$, when snow was fallen, and the amount of layers which affect it from above. It is assumed that in the moment of holding of snow depth measurement all the layers inside the column are in quasi-static equilibrium, i.e. experiencing only elastic deformation under gravity.

For determination of density of these layers formulae based on [Yosida, Huzioka, 1954] with consideration of empirical parameter responsible for changing of element's size under permanent deformation related to pressure of overlying elements [Epifanov, Osokin, 2010]) were used:

$$\rho = \frac{\frac{mg}{10^6(1-\sigma)} + 1.86}{0.0167}, T > -5^oC; \rho = \frac{\frac{mg}{10^6(1-\sigma)} + 10.8}{0.059}, T \leq -5^oC \tag{2}$$

where $m = H \cdot (\rho_1 + \rho_2 + \ldots), H = 0.01m$, $\rho_1.\rho_2, \ldots$ - densities of the first, second, etc. elements.

Obviously, during the process of snow accumulation, layers ('inclusions') will be distinguished in snow column, which have quite homogeneous density being determined in dependence on temperature (i.e. large layers formed at different temperature conditions of snow falling could be found).

If snow depth is stable for one day and further, the number of elements didn't change ($\triangle N = 0$). Provided no precipitation, snow density and SWE don't have variations; otherwise equal amount of moisture is added to each element.

In SMFE it is suggested that snow depth decrease ($\triangle N < 0$) is calculated on the basis of analysis of measured values of meteorological parameters: melting took place when there are positive temperatures during a day,

snow blowing – when there are negative temperatures in case of significant snow depth decrease; in other cases it is suggested that snow subsidence took place.

In case of snow subsidence mass redistribution between elements in all 'inclusions' is performed by sequential exclusion of layers with minimum density with their mass redistribution to all the layers until the measured snow depth value at a certain time will be achieved.

Mass of melted snow is defined regarding the decrease of the depth of snow cover with earlier determined density. Clear that a part of formed water is removed due to runoff and a part is redistributed is snow thickness. Following this assumption recalculation of density of each layer is made. In case of snow blowing a part of snow is also removed (although it breaks the general picture of the mass balance, however, 'move' the picture of simulated snow in accordance with the measurement data). Each time step in SMFE calculation of evaporation from snow is possible, according to [Kuzmin, 1961].

It is suggested that maximum snow density in the model doesn't exceed density of porous ice equal to about 700 kg/m^3.

Every day snow water equivalent $SWE_{(tk)}$ is calculated as a sum of densities ρ_n of all the layers and snow column density, $\rho_{(tk)}$ – as an averaged value of all the layers:

$$SWE(t_k) = \sum_{n=1}^{N(t_k)} \rho_{n(tk)}(t_k) \cdot h, \rho_{(tk)} = \frac{1}{N_{(tk)}} \sum_{n=1}^{N(t_k)} \rho_{n(t_k)}(t_k) \quad (3)$$

Computational algorithm of the model is realized in Fortran-90.

Reliable testing results of SMFE model were presented in [Kazakova, Chumakov, Rozinkina, 2013], which show good compliance with observations. Example of comparison of SWE measurements, SWE field based on SMFE and COSMO initial SWE field are shown in Fig.4.

4 SWE technology and snow density analysis (SNOWE technology)

On the basis of developed snow model was developed a technology for preparation of initial fields of SWE and snow density (SNOWE technology). The general scheme is presented on Fig.2. During the 'snow' season 2014/2015 the proposed technology was tested in quasi-operational mode at Hydrometcenter of Russia. Forecasts were produced starting from 00 UTC every day for two domains of COSMO-Ru model - for the territories of Central and East Europe and European part of Russia (COSMO-Ru7 - grid step 7 km) and for territory of Central Russia (COSMO-Ru2, grid step 2.2 km) (Fig.3).

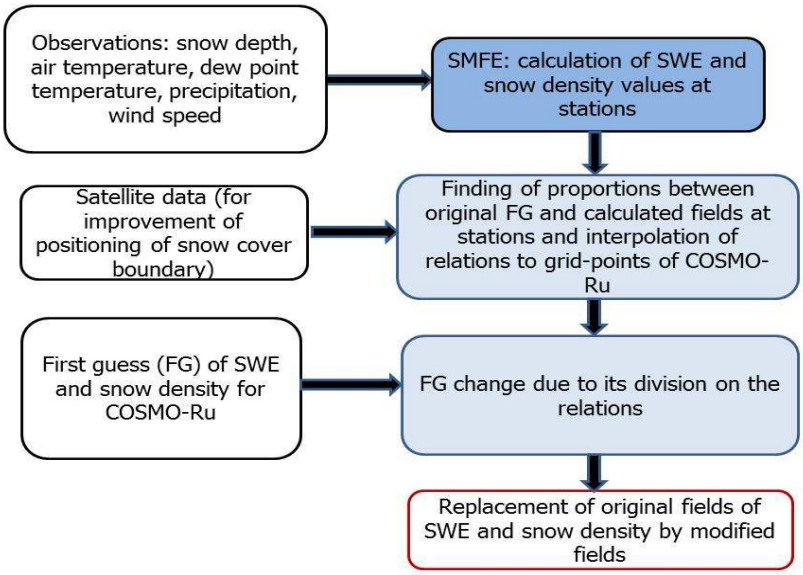

Figure 2: Technological scheme for preparation of initial fields of SWE and snow density at Hydrometcenter of Russia.

The SMFE model generates SWE and snow density values for stations based on daily SYNOP measurements.

Observations from 2296 stations were used for COSMO-Ru7 area, the quality control of snow depth and T2m measurements was performed.

As a first step for Objective Analysis (OA), the FG data (gridded values of SWE and snow density from initial data (based on the global DAS) for COSMO-Ru) is interpolated from COSMO-Ru grid points to the points of SMFE calculations (points of observations). For these points the proportions between COSMO-values and SMFE-values are determined. Than these relations are interpolated to the grid points of COSMO-Ru to correct the initial fields. The interpolation of obtained local values of proportions to the grid-points of COSMO model was realized on the basis of Delaunay triangulation. At this step satellite data with 4-km resolution from NOAA server (ftp://140.90.213.161/autosnow/4kmNH/) was used for improvement of positioning of snow cover boundary. Finally, the normalized FG of SWE and snow density are used as initial fields.

Tests demonstrated small differences between the results of direct interpolation of SWE values from SMFE to COSMO-grid and proposed OA technology in case of dense observational network (COSMO-Ru2).

The zone with maximum changes of meteorological elements during the 'snow period' is the zone close to the snow boundary, especially during snow melting. Changes in air temperature especially and other meteorological parameters will be viewed with changes of initial fields of SWE and snow density in this boundary zone.

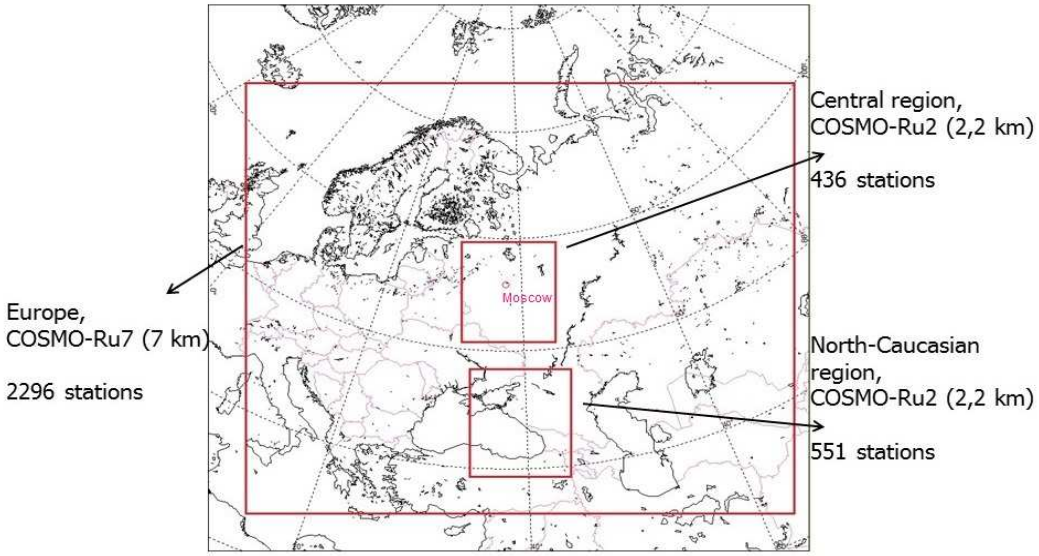

Figure 3: Regions of COSMO-Ru.

5 Verification of COSMO-Ru forecasts calculated operationally and according to SNOWE technology

Verification of results of the proposed technology was done in VERSUS mostly for spring period of snow melting period during 2014/2015 snow season.

Small improvement of RMSE of T2m COSMO-Ru7 forecasts in case of using the proposed technology can be observed (graphs were produced for approximately 800 stations). Such a result points to the fact that conditional verifications needed to reveal the expected effect, as the territory of COSMO-Ru7 region is large and snow boundary migrates daily.

An example of efficiency of new technology is shown on Fig.5. ME and RMSE values for air temperature for COSMO-Ru7 area were reduced (RMSE for 0,5-1,5^{o}C and ME for 0,5-1,0^{o}C), especially for the 3d day of the forecast (Fig.5-6). Errors in positive T2m forecasts are greater than in negative. Improvement in T2m forecasts using proposed technology is observed both for positive and negative T2m.

For Central Russia (COSMO-Ru2 model) such dependence can be recorded only through separate dates (Fig.7, Table 1) since the territory (area of integration) is not big enough to 'catch' moving of snow boundary during snow melting period.

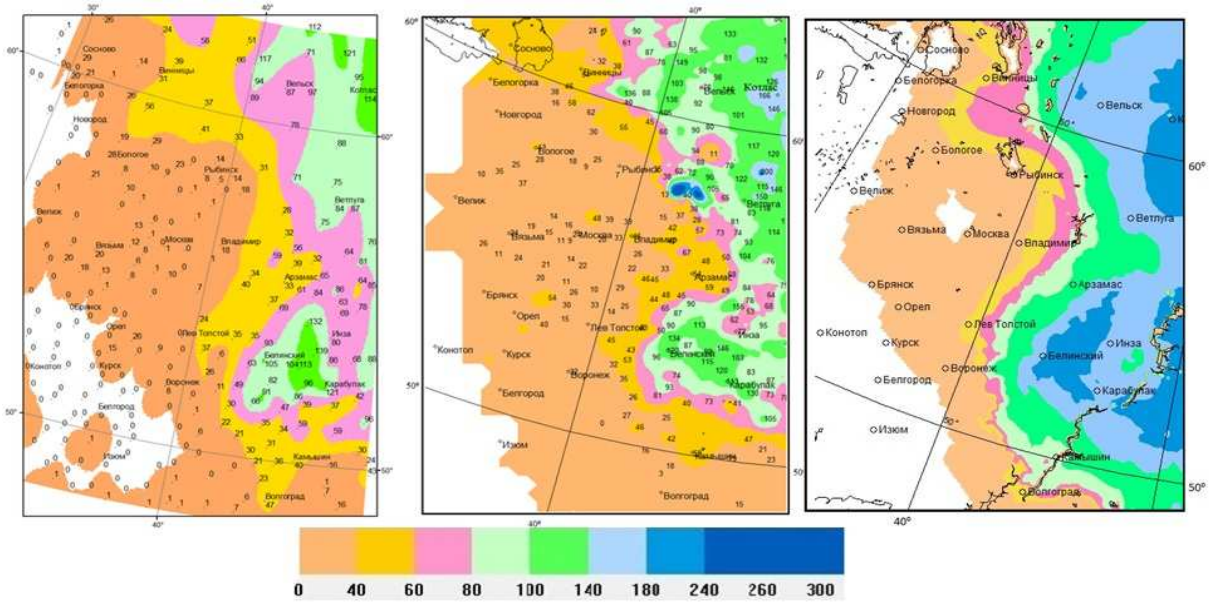

Figure 4: Maps of SWE (mm) obtained on the basis of SMFE calculations (left), with the help of graphical package 'GIS Meteo' by snow surveys' data (center) and SWE initial fields for COSMO-Ru7 (right). 28 Feb 2014.

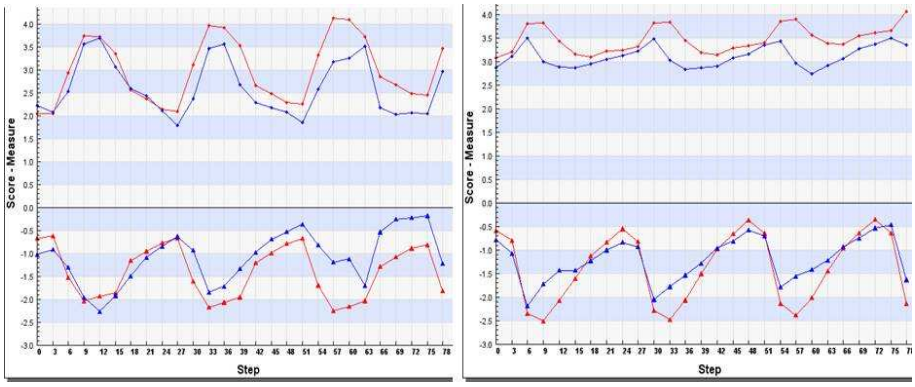

Figure 5: ME (bottom lines) and RMSE (upper lines) values for air temperature(^{o}) forecasts for the COSMO-Ru7 area according to operational (red dots) and experimental (blue dots) modes for 24 Feb-31 March 2015. Left- when positive air temperatures were observed at the stations, right-upon condition when negative.

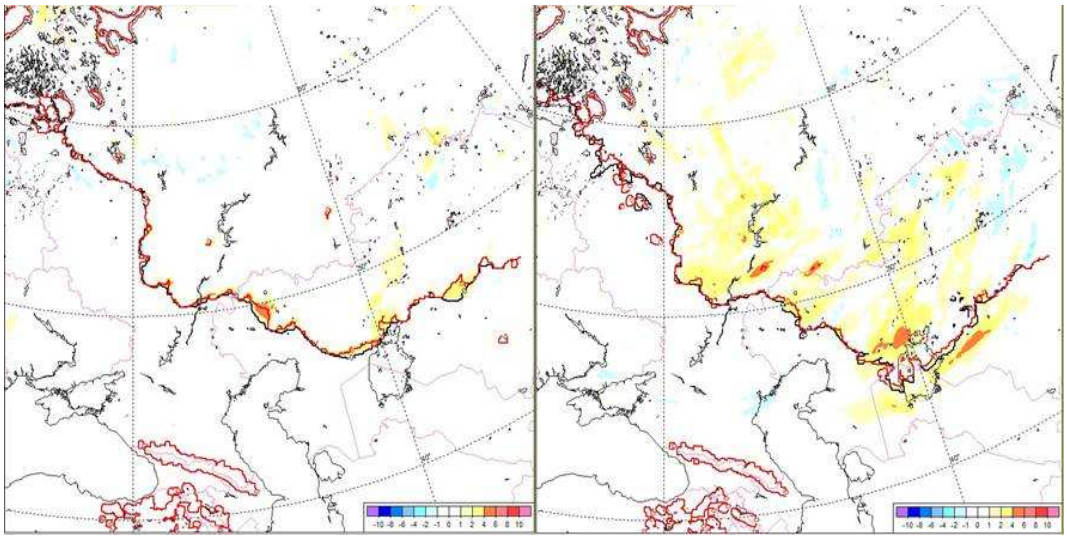

Figure 6: Difference between air temperature (^oC) forecasts at 12 UTC (left) and 78 UTC (right) for the COSMO-Ru7 area according to operational and experimental modes. 25 March 2015.

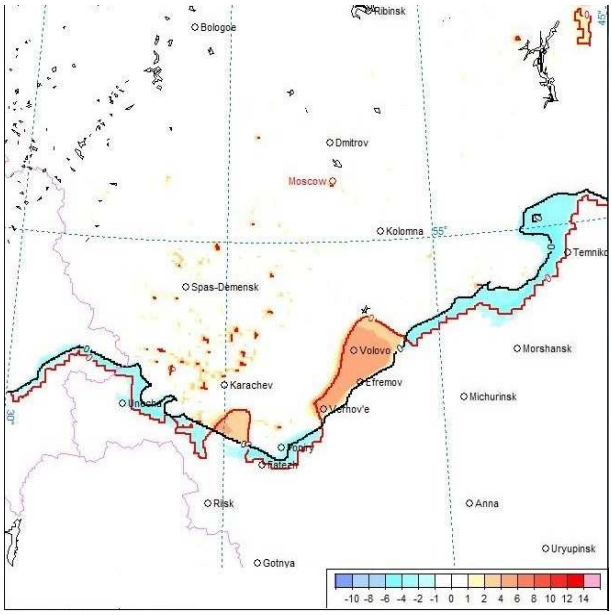

Figure 7: Difference between air temperature (^oC) forecasts at 12 UTC for the COSMO-Ru2 area (Central Russia) according to operational and experimental modes. 10 April 2013.

Table 1: T2m (^{o}) for 12 UTC and 00 UTC at stations situated close to the snow boundary according to observations and forecasts for 12 and 24 hours for operational and experimental modes of COSMO-Ru2 technology

	10 April 2013, 12 UTC			11 April 2013, 00 UTC		
Station	Obs t^oC	Operational mode t^oC / abs. error,°C accuracy%	Experiment t^oC /abs. error,°C accuracy%	Obs t^oC	Operational mode t^oC / abs. error,°C accuracy%	Experiment t^oC / abs. error,°C accuracy%
Efremov	8.1	4.3/ 3.7/0	6.6 /1.4/ 100	-0.4	-0.5/ 0.1/ 100	-0.6/ 0.2/ 100
Volovo	6.9	0.6/ 6.3/ 0	5.8 /1.1/ 100	-1.1	-3.6/ 2.5/ 100	-1.7/ 0.6/ 100
Verhov'e	7.0	1.2/ 5.8/ 0	6.0 /1.0/ 100	0.8	-1.2/ 2.0/ 100	-0.2/ 1.0/ 100
Temnikov	7.2	6.2/ 1.0/ 100	5.6 /1.6/ 100	0.2	0.7/ 0.5/ 100	-3.0/ 2.8/ 100
Unecha	7.1	6.6/ 0.5/100	5.4 /1.7/ 100	1.0	0.4/ 0.6/ 100	0.7/ 0.3/ 100
Fatezh	8.1	5.6/ 2.5/100	6.7 /1.4/ 100	-1.5	-3.0/ 1.5/ 100	0.3/ 1.8/ 100
Mean abs. error, °C / mean accuracy,%		3.3°C /50%	1.4°C /100%		1.2°C / 100%	1.1°C / 100%

Comparing T2m forecasts for the case with significant cloudiness- total cloud cover($TCC \geq 75\%$, overcast) with the case of insignificant prognostic cloudiness ($TCC \leq 25\%$, clear sky) the proposed technology provides some differences in their prognostic values for the first day of the forecast shown at Fig.8.

It can be related to the local TCC changes in the COSMO-model. If we take into account both prognostic and observed values of TCC Fig.9), significant improvements of RMSE and ME are observed for clear sky both for positive and negative values of observed T2m (Fig.9-11). For forecasts when $TCC \geq 75\%$ improvement of RMSE for positive temperatures occurs for 2-3 forecast days, for negative - it is not so pronounced (RMSE decreases, ME increases). Proposed technology improves T2m forecasts for cases of mostly positive T2m at clear sky conditions.

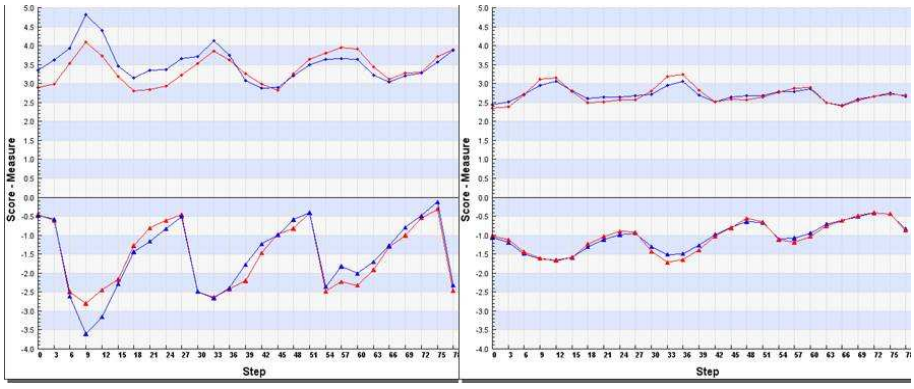

Figure 8: ME (bottom lines) and RMSE (upper lines) values for air temperature (^{o}C) forecasts for the COSMO-Ru7 area according to operational (red dots) and experimental (blue dots) modes for 24 Feb-31 March 2015. Left-upon condition that prognostic $TCC \leq 25\%$, right-upon condition it was $\geq 75\%$.

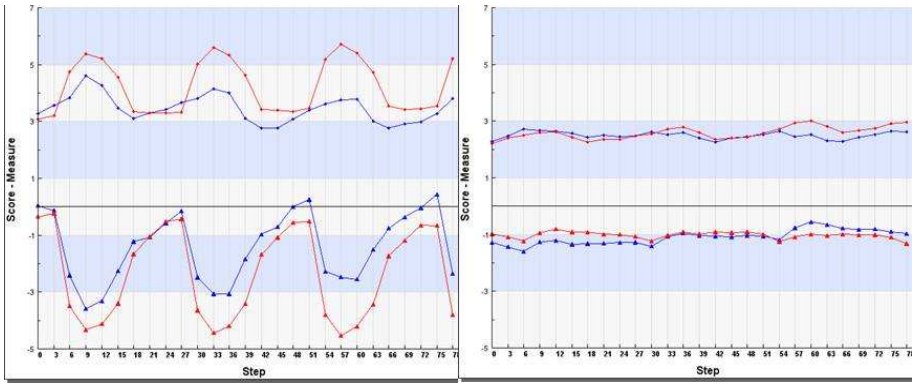

Figure 9: ME (bottom lines) and RMSE (upper lines) values for air temperature (^{o}C) forecasts for the COSMO-Ru7 area according to operational (red dots) and experimental (blue dots) modes for 24 Feb-31 March 2015. Left-upon condition that both prognostic and observed TCC was $\leq 25\%$, right-upon condition that it was$\geq 75\%$.

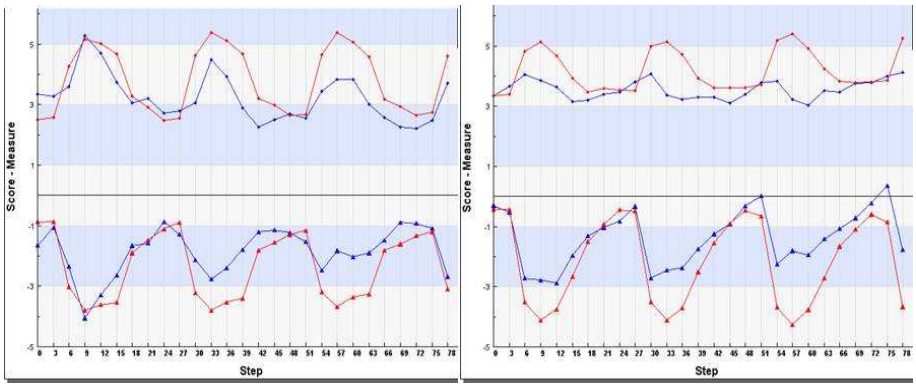

Figure 10: ME (bottom lines) and RMSE (upper lines) values for air temperature (^{o}C) forecasts for the COSMO-Ru7 area according to operational (red dots) and experimental (blue dots) modes for 24 Feb-31 March 2015. Left-upon conditions that prognostic TCC was $\leq 25\%$ and positive air temperatures were observed at stations, right-upon condition that TCC was $\geq 75\%$ and negative air temperatures were observed at stations.

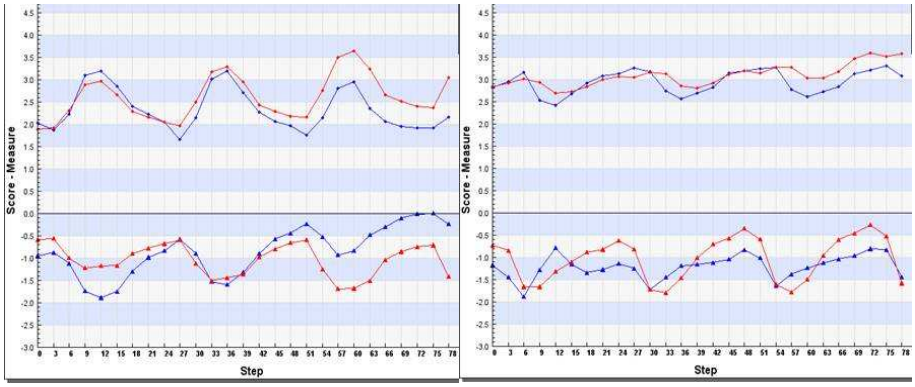

Figure 11: ME (bottom lines) and RMSE (upper lines) values for air temperature (°C) forecasts for the COSMO-Ru7 area according to operational (red dots) and experimental (blue dots) modes for 24 Feb-31 March 2015. Left-upon conditions that prognostic TCC was $\geq 75\%$ and positive air temperatures were observed at stations, right-upon condition that TCC was $\geq 75\%$ and negative air temperatures were observed at stations.

Changes in improvement T2m forecasts are observed both for COSMO-Ru2 and COSMO-Ru7 technologies when snow is present (Fig.12). The thinner snow cover is (case of snow depth ≤ 5 cm), the more probability we have that it will melt during the forecast time (see decreasing of RMSE and ME in time scale in Fig.12).

Consequently, the main conclusion follows from verification of T2m COSMO-model forecasts using the proposed technology with modified initial SWE and snow density fields, is that the largest improvement of T2m forecasts is in case of positive temperatures under clear sky conditions, and thin snow cover, i.e. in the areas close to snow boundary.

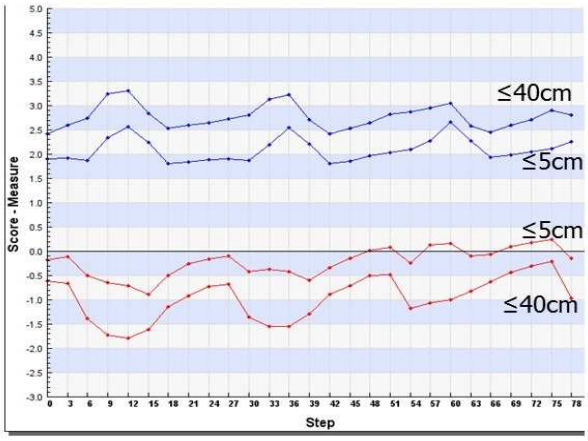

Figure 12: ME (red lines) and RMSE (blue lines) values for air temperature (°C) forecasts for the COSMO-Ru7 area according to experimental mode upon conditions that prognostic snow depth ≤ 5 cm and ≤ 40 cm for 24 Feb-31 March 2015.

Differences between two technologies in TCC forecasts are mostly observed on cloud edges and in the zones of rare cloudiness (Fig.13).

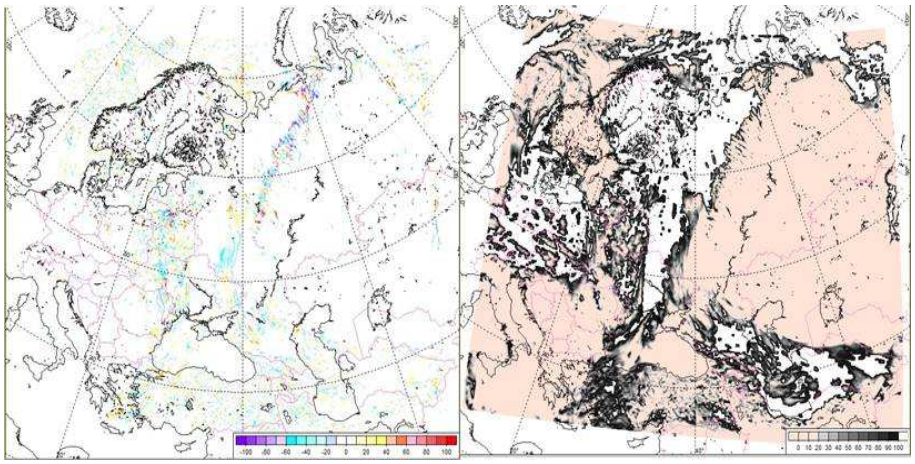

Figure 13: TCC (%) forecast at 12 UTC for the COSMO-Ru7 area according to experimental mode of COSMO-Ru7 (right) and its difference with operational mode (left). 31 March 2015.

When modifying initial fields of SWE and snow density, prognostic values of these snow characteristics will also be changed (Fig.14). Differences in albedo between two technologies will be observed in area close to the snow boundary (Fig.15). Albedo and TCC modifications will affect the radiative balance and, hence changes in heat fluxes occure (see example in Fig.16).

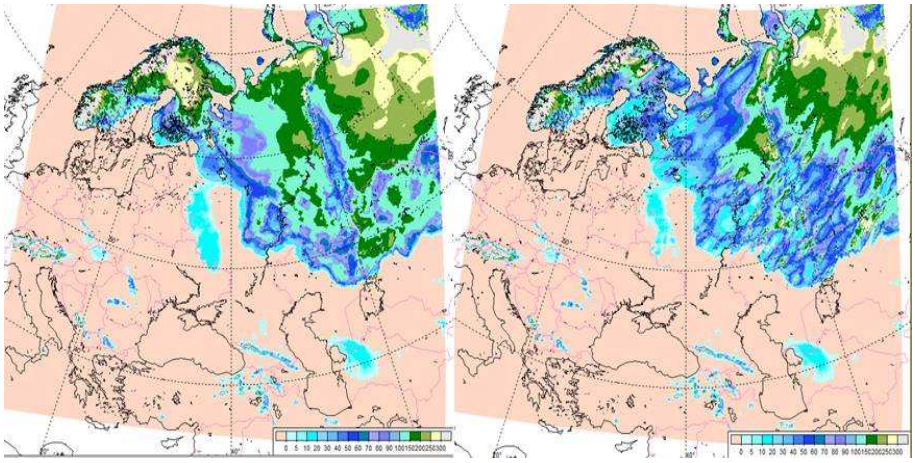

Figure 14: SWE (mm) forecasts at 12 UTC for the COSMO-Ru7 area according to operational (left) and experimental (right) modes of COSMO-Ru7. 31 March 2015.

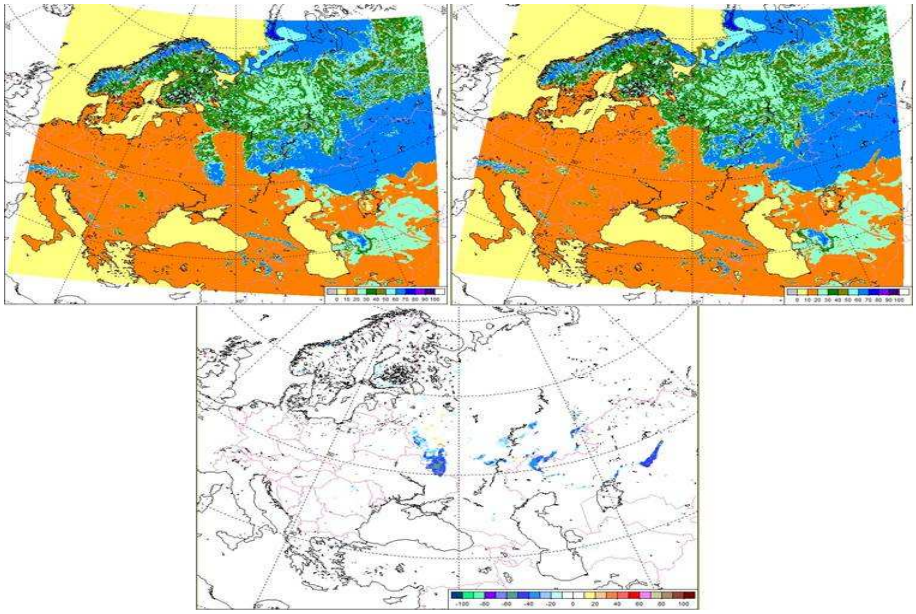

Figure 15: Albedo (%) forecasts at 12 UTC for the COSMO-Ru7 area according to operational (left) and experimental (right) modes of COSMO-Ru7. Bottom-difference between experimental and operational modes. 31 March 2015.

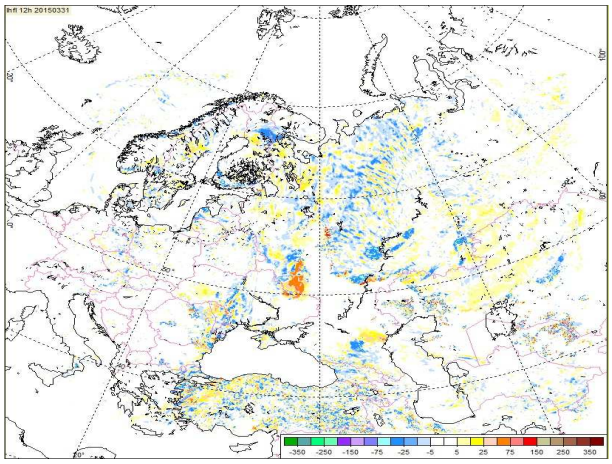

Figure 16: Difference between latent heat flux (W/m^2) forecasts at 12 UTC for the COSMO-Ru7 area according to operational and experimental modes of COSMO-Ru7. 31 March 2015.

Changes in 10 m wind speed forecasts using the proposed technology can be detected only locally, the graphs for errors between two technologies don't give specific differences (Fig.17). Assessment of ME and RMSE for 10m wind speed in positive air temperature range observed at stations doesn't show clear advantage of proposed technology. RMSE decrease at 18-24 UTC (especially for the 3d day of the forecast) while ME increase.

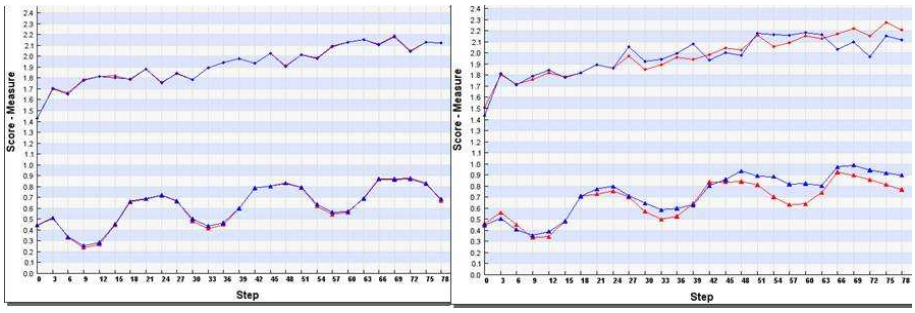

Figure 17: ME (bottom lines) and RMSE (upper lines) values for 10m wind speed (m/s) forecasts for the COSMO-Ru7 area according to operational (red dots) and experimental (blue dots) modes for 24 Feb-10 April 2015. Right-upon condition that positive air temperatures were observed at stations, left-without conditions.

Thus, local changes in forecasts of 10 m wind speed and cloudiness were also found, however distribution of special patterns of their occurrence were not indicatively diagnosed. It is demonstrated that modifications in initial fields of SWE and snow density are consistent with the standard COSMO forecast and lead to improvements of surface variables' forecast (especially T2m).

Conclusions

The SNOWE technology was realized in operational technologies COSMO-Ru for the winter of 2014/2015. The implementation of SNOWE technology showed the positive impact for SWE forecasts as well as for T2m forecasts near the snow boundary. The more realistic forecast of SWE based on the SNOWE corrected initial data provides more realistic speed of movements of snow boundary during the forecast time.

The largest improvement (2-3^{o}C after averaging and up to 7^{o}C for particular cases) is observed for T2m forecasts in the cases of clear sky conditions and cases with thin snow cover. Some influence is indicated for total cloud cover, 10m wind speed forecasts as well as for heat fluxes and surface albedo.

References

[1] Bartlett P.A, MacKay M.D., Verseghy D.L., 2006. Modified Snow Algorithms in the Canadian Land Surface Scheme: Model Runs and Sensitivity Analysis at Three Boreal Forest Stands. Atmosphere-Ocean, Canadian Meteorological and Oceanographic Society, 43 (3), **207-222**.

[2] Epifanov V., Osokin N., 2010. Research of strength properties of snow on a mountain slope of the Spitsbergen archipelago. Earth's cryosphere, vol. XIV, No.1, **81-91** (in Russian).

[3] Kazakova E., Chumakov M., Rozinkina I., 2013. Realization of the parametric snow cover model SMFE for snow characteristics calculation according to standard net meteorological observations. COSMO Newsletter, No.13, **39-49**.

[4] Kazakova E., Rozinkina I., 2011. Testing of Snow Parameterization Schemes in COSMO-Ru: Analysis and Results. COSMO Newsletter, No.11,**41-51**.

[5] Kuzmin P. Process of Snow Cover Melting. Leningrad, Hydrometeoizdat, 1961, **345** (in Russian).

[6] Yosida Z., Huzioka T., 1954. Some Studies of the Mechanical Properties of Snow. IAHS Red Book Series. Publ. no. 39, Gentbrugge, **98-105**.

Running the COSMO model on unusual hardware architectures

Davide Cesari

Arpae-SIMC, Bologna, Italy

1 Introduction

Nowadays more and more objects around us contain a computer, or simply *are* a computer, with a processor, some amount of memory and network capabilities, qualitatively analogous to those of a desktop computer or of an HPC (High Performance Computing) system. Moreover, many of these objects ("devices") are based on the Linux operating system and are capable to run executable codes generated by the gcc (GNU Compiler Collection), which includes the gfortran compiler that many of us use to compile the COSMO model. It is thus natural to ask oneself: could I run my favourite NWP model on such a device? The answer is yes, as it can be seen in the following sections.

2 Choice of the device

The most obvious choice of a device for this test would have been an Android smartphone, since these devices are nowadays rather powerful, universally widespread, and Android runs on top of a Linux kernel. However the commercial Android devices come with many barriers related to security and industrial secrets, so that it is possible to run arbitrary executables only after performing some hacking procedures (so-called "rooting" of the phone), which are risky and potentially illegal. For this reason a more open platform has been chosen: it is a fairly cheap (≈150 EUR) satellite receiver based on a MIPS processor and the Enigma2 TV interface on top of a basic Linux installation. The mass storage device consists in an external USB disk. The ultimate reason for this choice is simply that two of these devices are present in the author's home, see fig 1. An overview of the technical specifications of the devices is presented in table 1. The website of the manufacturer is http://www.gigablue.de.

Model	Processor	Memory
Gigablue 800 UE	333 Mhz Brcm4380	104 MB
Gigablue 800 SEplus	750 Mhz Broadcom BMIPS3300	222 MB

Table 1: Characteristics of the devices used for the test.

3 Preparing the model executable

Since this kind of devices has usually a limited amount of memory and of precompiled software packages available, it is hard to compile a complex Fortran code like the COSMO model on the device itself. Thus it has been decided to adopt the technique known as *cross-compiling*, which consists in generating the executable for the target architecture on a computer having a different architecture, reasonably a desktop computer. The Debian GNU/Linux distribution for traditional desktop computers is very suitable for this purpose, because it provides pre-compiled packages of gfortran compiler, with support for cross-compiling to many different target architectures

The instruction about how to setup a cross-compiling environment are described on a specific page of the Debian web site [1] and they can be resumed in four simple commands to be run by root on an installed system:

```
dpkg --add-architecture mipsel
apt-get update
apt-get install crossbuild-essential-mipsel
apt-get install gfortran-mipsel-linux-gnu
```

where `mipsel` indicates the MIPS architecture chosen for this particular test, so it may vary depending on the device chosen. After this step, a full set of compiling and linking commands becomes available on the system, simply by prefixing the usual command name (e.g. `gfortran`, `gcc`, `ar`) by the target-specific prefix, in this case `mipsel-linux-gnu-`.

For simplifying the task of compiling the COSMO model, it has been decided to build a sequential executable, without MPI and with only the DWD grib1 library, thus without the external libraries grib_api and netcdf. This step may require some editing of the COSMO code, depending on version, because such a combination is not well tested.

Moreover, a static executable has been built, in order to avoid problems related to possibly different system libraries between the cross-compiling system and the target system.

Thus, for performing cross-compilation, in the libgrib1 makefile and in COSMO `Fopts` file, the cross-compiling commands with the special prefix have been specified in place of the ordinary commands, such as mipsel-linux-gnu-gfortran for the Fortran compiler and linker. The COSMO makefile target used for this type of test has been `purseq`, i.e. sequential executable without assimilation and RTTOV code.

The flexible structure of the GNU gcc/gfortran compiler has proven to be very useful for this compilation task. The compiling process in gcc takes place in three main stages: a language-dependent and platform-independent front-end stage, which translates the program source code into an universal meta-language, a common optimisation stage and a final platform-dependent backend stage, where the object code is generated [2].

This structure allows to compile on different platforms with a minimum of changes in the command line and with access to almost the same set of optimisations.

4 The test case

Due to the small amount of memory available on the device used, it has been chosen to run a 3-dimensional test run on a very small grid. In order to make the test simpler and easily portable, the test has been configured to use artificial initial, boundary and external data.

The setup has been chosen among the test configurations available in the COSMO code and implemented by Ulrich Blahak [3]. The domain size used was $21 \times 21 \times 40$ grid points with 2km of grid step and 12s of time step. The initial state was characterized by a positive temperature anomaly in the center of the domain ("warm bubble").

Figure 1: Image of the Gigablue 800 UE used for one of the tests.

5 Performing the tests

Since the basic operating system in the devices under test is a plain GNU/Linux system, the procedure of running COSMO on this kind of system does not differ from what we are used to: opening a terminal on a personal computer, connecting to the device over the network with ssh and starting an executable from the command line. Unfortunately these particular devices do not have a console on the local TV screen, thus it is not possible neither to log in from the device itself, nor to have any feedback, on the TV screen, of the fact that a complex NWP model is running.

6 The results

The test case described above has been run on the two MIPS platforms described and, for comparison, on a state of the art HPC computing node (price ≈2000 EUR) using a single processing core.

The numerical results of the tests have shown only minor mutual discrepancies, within acceptable limits for this kind of simulations.

Table 2 summarises the results of the tests in terms of total wall-clock time required for one hour of forecast with the configuration described, as reported in the YUTIMING file.

Platform	wall clock time (s)
Gigablue 800 UE	1111
Gigablue 800 SEplus	28649
HPC computing node	12

Table 2: Summary of the tests performed.

The 800 SEplus model, although being more recent, has shown very poor performances because its processor lacks a FPU (Floating Point Unit), so the usual floating point operations with Fortran real numbers, which account for most of the COSMO model computing time, are emulated by the operating system using several integer operations per single floating point operation.

The 800 UE, equipped with a FPU, shows much better performances, although still being two orders of magnitude slower than a state of the art high performance computing platform. Even considering the smaller power consumption and price of the MIPS platform, the HPC node still wins in terms of performance per Watt and performance per price.

7 Conclusions

Since the computational resources required by the run of a state of the art operational NWP model are much higher than what can be provided even by a single node of an HPC system, it is clear that there is no use for such small devices for practically running a code like the COSMO model. And this is even more true when considering the relatively low parallel scalability potential of such devices.

However the feasibility of such an operation, through cross-compiling, has been proved and one key to the success has been the flexible structure of the free gcc/gfortran compiler.

Next step will be setting up cross-compilation with external dynamic libraries, including MPI, and trying a multiprocess run with MPI on a cheap multi-core minicomputer with arm architecture, like the Raspberry-Pi.

References

[1] CrossToolchains - Cross-compiling on Debian GNU/Linux.https://wiki.debian.org/CrossToolchains.

[2] GNU Compiler Collection, Wikipedia.https://en.wikipedia.org/wiki/GNU_Compiler_Collection

[3] Blahak, U., 2015: Simulating idealized cases with the COSMO-model. Available online.http://www.cosmo-model.org/content/model/documentation/core/artif_docu.pdf, **48**.

COSMO-based ensemble forecasting for Sochi-2014 Olympics: archiving the results

Elena Astakhova1, Andrea Montani2, Dmitry Kiktev1, Alexander Smirnov1

1 Roshydromet, Moscow, Russia 2 ARPA–SIMC, Bologna, Italy

1 Introduction

The last winter Olympic/Paralympic Games were held in February-March 2014 in Sochi, Russia. The Russian Meteorological Service (Roshydromet) initiated a special international project FROST-2014 (FROST - Forecast and Research in the Olympic Sochi Testbed) related to these Games; it got a status of WMO World Weather Research Programme (WWRP) blended Forecast Demonstration and Research and Development Project (Kiktev et al., 2015a; Kiktev et al., 2015b).

The COSMO activity in FROST-2014 was integrated within a consortium priority project Consolidation of Operation and Research results for the Sochi Olympic Games (PP CORSO) (Rivin and Rozinkina, 2013). PP CORSO finished in 2014. Its results included a successful experience of high-resolution modeling in mountainous areas, improved downscaling/postprocessing procedures for the Sochi region, regular provision of probabilistic forecasts during the Games as well as research in ensemble modeling with different resolutions.

It was realized in 2014 that some additional work was necessary to implement CORSO achievements to COSMO practice and to enable their better usage. That is why the priority task CORSO-A followed PP CORSO. Here only the ensemble component of CORSO and CORSO-A activity will be considered. We shall briefly remind CORSO results, overview the goal of CORSO-A, and summarize its results.

2 Ensemble prediction systems developed in CORSO

Two ensemble prediction systems (EPS) were developed within PP CORSO: COSMO-S14-EPS with a 7-km resolution and COSMO-Ru2-EPS with a 2.2 km resolution (Montani et al, 2013, 2014, 2015). COSMO-S14-EPS (S14 stands for Sochi2014) was created at ARPA-SIMC (Montani et al, 2013) and was a version of COSMO-LEPS system (Montani et al, 2011) displaced from the European area to the Sochi region.

The system was driven by the ECMWF EPS, namely, by its most representative prognostic realizations which were selected by a clustering procedure. The lower boundary condition was a result of COSMO model run in hindcast mode (a short-range forecast nested on ECMWF analyses).

The model-related uncertainties were taken into account in COSMO-S14-EPS by using two different convection parameterization schemes (Tiedtke or Kain-Fritsch, random choice) in different members and also by varying tuning coefficients in parameterizations of sub-grid scale processes (in particular, turbulent). The most essential differences between COSMO-S14-EPS and COSMO-LEPS systems were integration domains (Sochi region or Europe) and ensemble sizes (10 or 16 members, respectively).

The system with a 2.2-km grid size named COSMO-Ru2-EPS ran at Roshydromet and performed a dynamical downscaling of COSMO-S14-EPS increasing the forecast resolution both in horizontal (from 7 to 2.2 km) and in vertical (from 40 to 50 levels).No additional perturbations were introduced neither to initial and boundary conditions nor to the model.

The ensemble has the same size as in COSMO-S14-EPS and was composed of 10 perturbed members with no control. Both EPSs ran operationally during the Olympics/Paralympics, their results were provided to Sochi forecasters and proved to give a valuable support to them.

In fact, the entire length of parallel runs of COSMO-S14-EPS and COSMO-Ru2-EPS was longer than the period of the Games and covered December 2013-April 2014. The forecast results were archived on Roshydromet servers along with initial and boundary conditions generated by COSMO-S14-EPS and later used by COSMO-Ru2-EPS.

3 CORSO-A necessity and goal

It is worth to note here that COSMO ensemble forecasts can be considered a part of a more extensive FROST-2014 archive that included the results of four more ensemble prediction systems (Kiktev et al, 2015; Astakhova et al, 2015).

The two systems, GLAMEPS and HarmonEPS, were presented to FROST-2014 by the Norwegian Meteorological Institute, while ALADIN-LAEF and NMMB-EPS came from the Central Institution for Meteorology and Geodynamics (ZAMG), Austria, and the National Centers for Environmental Prediction (NCEP), USA, respectively.

The EPS resolution was 7 to 11 km except for the convection permitting HarmonEPS with its 2.5 km horizontal step; the ensemble size varied from 7 to 54. Additionally, deterministic forecasts by 9 different systems, nowcasts from 6 systems, and a variety of observational data of different types, including station, radar, profiler data, operational meteorological bulletins, camera snapshots, etc., were aggregated at the FROST-2014 server and available via the project web-site $http://frost2014.meteoinfo.ru$.

By no doubt, this huge amount of forecast and observation data could be very useful for research in the field of short-range limited-area deterministic and ensemble prediction. Remember that the Sochi area is a very complex region with steep mountains lying near the warm Black Sea and forecasting in mountainous regions is still a challenge for numerical weather prediction models.

However, it became clear after the Olympic Games, that in research tasks it would be quite difficult and problematic to use the forecast data in the form presented on the FROST-2014 server because of different coding and organization of data files transferred to Roshydromet by various data providers.

The application of the archive would be much easier if the forecast data were organized following some standard rules. A good idea is to follow TIGGE-LAM project and to prepare a Sochi unified archive using the coding standards and user interfaces adopted in TIGGE-LAM (Paccagnella et al., 2012). TIGGE and TIGGE-LAM data portals are well known and very popular in scientific community and a lot of research has been done using the data presented there.

That is why one of CORSO-A goals was to implement a unified archive of COSMO ensemble forecasts (with 7 and 2.2 km resolutions) for the Sochi area. The archive was expected to be accompanied by the data on initial and boundary conditions for high-resolution ensembles and by a list of important weather events during Olympics and Paralympics.

4 A Unified Sochi archive

The Sochi unified archive covers the period from January 15, 2014 to March 16, 2014. This time interval coincides with the period adopted for verification in FROST-2014 (January 15 - March 15, 2014). The archive contains the ensemble forecasts by COSMO-S14-EPS and COSMO-Ru2-EPS starting at 00 UTC and 12 UTC on the dates within the above-mentioned two-month interval.

The prognostic fields for all members are presented with a 3h time frequency on the original COSMO-model rotated latitude-longitude grid with resolutions 7 and 2.2 km for COSMO-S14-EPS and COSMO-Ru2-EPS, respectively. The accumulated parameters (precipitation and wind gusts at 10 m) are not archived at zero timestep. The data are in WMO-GRIB2 format. The archived parameters and the corresponding coding information are listed in **Table 1**.

The parameter set is slightly different from the TIGGE-LAM high-priority parameters. The Sochi archive does not contain large-scale precipitation, convective inhibition, and convective available potential energy. As static fields (land-sea mask and orography) did not change during the period, they were written to the archive only once.

Table 1: Specification of Sochi archive

Parameter	Abbre-viation	Level	Units	GRIB2 specifics
10 metre U-velocity	10u	10m (103.10)	m s-1	Instantaneous Product Discipline 0 Parameter Category 2 Parameter number 3 paramId 165
10 metre V-velocity	10v	10m (103.10)	m s-1	Instantaneous Product Discipline 0 Parameter Category 2 Parameter number 2 paramId 166
Mean sea level pressure	msl	MSL (101)	Pa	Instantaneous Product Discipline 0 Parameter Category 3 Parameter number 0 paramId 151
Surface air temperature	2t	2m (103.2)	K	Instantaneous Product Discipline 0 Parameter Category 0 Parameter number 0 paramId 167
Surface air dew point temperature	2d	2m (103.2)	K	Instantaneous Product Discipline 0 Parameter Category 0 Parameter number 6 paramId 168
Accumulated precipitation (liquid+frozen, convective+large-scale)	tp	surface (1)	kg m-2	Accumulated from the beginning of the forecast Product Discipline 0 Parameter Category 1 Parameter number 52 paramId 228228
10 metre wind gust in the last 3 hours	10fg3	10m (103,10)	m s-1	Product Discipline 0 Parameter Category 2 Parameter number 22 typeOfStatisticalProcessing 2 paramId 228028
Orography (geopotential height at the surface)	orog	surface (1)	gmp	Instantaneous Control run Product Discipline 0 Parameter Category 3 Parameter number 5 paramId 228002
Land-sea mask	lsm	surface (1)	Propor-tion (0-1)	Instantaneous Control run Product Discipline 2 Parameter Category 0 Parameter number 0 paramId 172

The following ensemble meta-data information is included to the GRIB files

- the ensemble size (GRIB key numberOfForecastsInEnsemble)
- the number of ensemble member (GRIB key perturbationNumber)
- the forecast type (GRIB key dataType = pf/cf, i.e. perturbed/control)

No data for mean sea level pressure is available for COSMO-S14-EPS. Initial and boundary conditions for high-resolution COSMO EPS are available on demand.

All other FROST-2014 forecast data (both deterministic and ensemble) in the Sochi unified archive are coded in the same way. The archive is available at $http : /frost2014.meteoinfo.ru$ (authorization required). To download the forecasts, you must switch to Forecasts (upper panel) -Export of gridded ensemble forecasts (right panel), and then select the necessary data using the interface similar to that of TIGGE-LAM data portal (Fig. 1). The necessary data will be prepared in compressed form, the corresponding reference will be sent by e-mail, and then the data can be downloaded.

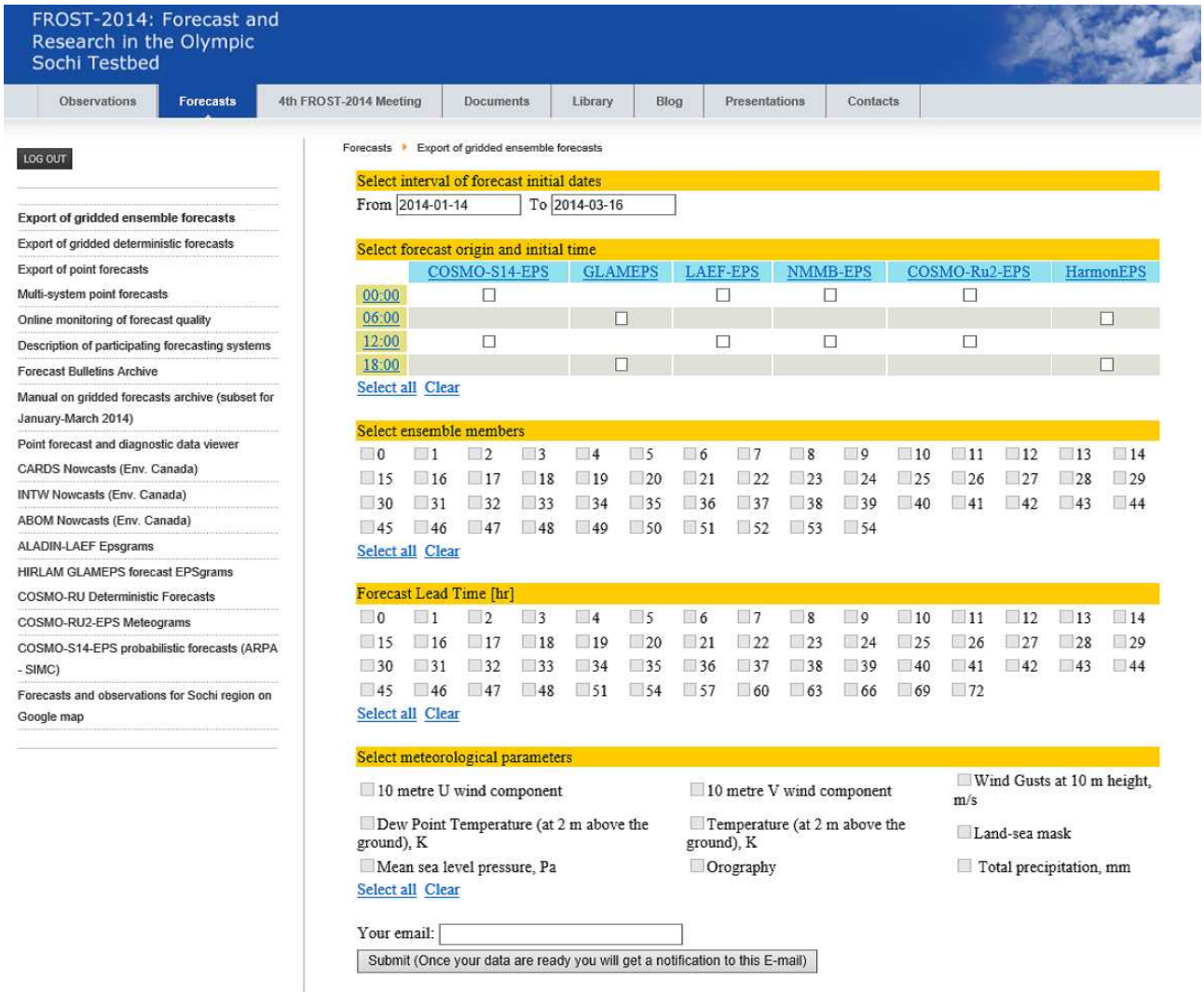

Figure 1: The FROST-2014 Web-interface used to download forecasts from the unified Sochi archive

Table 2: The most interesting cases during the Olympics/Paralympics

Case	Meteorological process/phenomenon	Models' behavior	Impact on competitions
07.02	Foehn	Poor temperature forecast (underestimated by 1.4-3.7^{o}C) by most models at Biathlon Stadium	
10-11.02	Dissipated precipitation	Precipitation in the Mountain Cluster predicted by the majority of systems, but not observed actually	
15.02		Poor forecast of maximum wind speed by most models at Krasnaya Polyana (underestimated by 3.5-7 m/s)	
16.02	Low visibility		Postponed competitions at Laura and Extreme Park
18.02	Cold front	Good precipitation forecast by most models	
22.02	Foehn	Poor temperature forecast by most models (negative forecast errors: -2.4 $-$ -4.4 ^{o}, most markedly at 1500 m)	
11.03	Cold front. Low visibility	Bad description of the behavior of maximum temperature (Tmax) by most models (Tmax forecasted at noon, whereas in reality it was observed in the morning)	Postponed skiing competitions at Roza Khutor
13.03		Poor precipitation forecast by most models above 1500 m	
17.03	Cold front	Underestimation of maximum wind speed by most models above 1500 m	

In addition to the prognostic fields, point forecasts (mean for ensembles) can be exported in csv format for more than 30 stations in the Sochi region. During the Olympics these forecasts were regularly presented at the multi-system page of the FROST-2014 site along with observation data and were considered very useful both by forecasters and researchers. To prepare these forecasts, the nearest grid-point approach was applied. A Web-tool to export observation data was also developed. For more details, please visit *http* : */frost*2014.*meteoinfo.ru*, where you will also find a short description of all FROST-2014 numerical weather prediction systems.

When research deals with the investigation of the skill of different weather prediction systems and of new ways to improve the forecast, it is important to have information about the synoptic situation in the analyzed domain and to select really essential events for case studies. To facilitate research in the field of short-range forecasting, Sochi forecasters prepared a list of cases recommended for detailed consideration. This list supplements the unified archive and is given in **Tab2**.

4 Conclusions

The unified Sochi archive containing forecasts for the area of Olympic Games 2014 for the period from January 15, 2014 to March 16, 2014 was prepared. The forecasts of two COSMO-based ensemble prediction systems, COSMO-S14-EPS and COSMO-Ru2-EPS with resolutions 7 and 2.2 km respectively, are stored in the archive.

The Web-tool to download the forecasts and observations as well as the list of interesting cases for research supplement the archive. The archive is organized in TIGGE-LAM style and is available at *http* : *//frost*2014.*meteoinfo.ru*. This work was carried out within the COSMO PT CORSO-A and WWRP FDP/RDP FROST-2014.

Acknowledgements

The authors are grateful to Tatiana Dmitrieva, Roshydromet, for providing the information on weather cases during the winter 2014 and to Tiziana Paccagnella, ARPA-SIMC, for supporting the work.

References

[1] Astakhova E. D., Montani A., Alferov D.Yu., 2015. Ensemble forecasts for the Sochi-2014 Olympic Games. Russian meteorology and hydrology,vol.40, iss.8,**531-539**. DOI 10.3103/S1068373915080051

[2] Kiktev D.B., Astakhova E.D., Zaripov R.B.,Murav'ev A.V.,Smirnov A.V., and TsyrulnikovM.D., 2015a.*FROST-2014 project and meteorological support of the Sochi-2014 Olympics.*Russian Meteorology and Hydrology, vol.40, iss.8,**504-512**. DOI 10.3103/S1068373915080026

[3] Kiktev D.B., Astakhova E.D., Zaripov R.B.,Murav'ev A.V,Smirnov A.V, and TsyrulnikovM.D., 2015b. Erratum to: *"FROST-2014 project and meteorological support of the Sochi-2014 Olympics"*, Russian Meteorology and Hydrology,vol.40, iss.12, **844–845**. DOI 10.3103/S1068373915120109

[4] Montani A., Cesari D., Marsigli C., Paccagnella T., 2011. Seven years of activity in the field of mesoscale ensemble forecasting by the COSMO-LEPS system: main achievements and open challenges. Tellus A, 2011,vol 63, **605–624**. DOI: 10.1111/j.1600-0870.2010.00499.

[5] Montani A., Marsigli C., Paccagnella T., 2013. Development of a COSMO-based limited-area ensemble system for the 2014 Winter Olympic Games. COSMO Newsletter, No. 13.**93–99** Available at *http* : *//cosmo − model.org/content/model/documentation/newsLetters/newsLetter*13/*cnl*13$_1$2.*pdf*

[6] Montani A., Alferov D., Astakhova E., Marsigli C., and Paccagnella T., 2014. Ensemble forecasting for Sochi-2014 Olympics: the COSMO-based ensemble prediction systems. — COSMO Newsletter, 2014, No. 14,**88–94**. Available at *http* : *//cosmo − model.org/content/model/documentation/newsLetters/newsLetter*14/*cnl*14$_1$0.*pdf*

[7] Montani A., Alferov D., Astakhova E., Marsigli C., Paccagnella T., 2015. Performance of the COSMO-based ensemble systems during Sochi-2014 pre-Olympics. COSMO Newsletter, 2015, No. 15, **77–82**. Available at *http* : *//cosmo − model.org/content/model/documentation/newsLetters/newsLetter*15/*cnl*15$_1$0.*pdf*

[8] Paccagnella T., Hacker J., Marsigli C., Montani A., Pappenberger F., Parsons D., Swinbank R., Toth Z., 2012. " THORPEX Interactive Research Grand Global Ensemble - Limited Area Model Plan" , WMO publications, THORPEX No 17, available at: *http* : *//www.wmo.int/pages/prog/arep/wwrp/new/wwrp*$_p$*ublications.html*

[9] Rivin G., Rozinkina I., 2013. Priority Project "CORSO": Consolidation of Operation and Research results for the Sochi Olympic Games. Available at *http* : *//cosmomodel.org/content/tasks/priorityProjects/corso/default.htm*

List of COSMO Newsletters and Technical Reports

(available for download from the COSMO Website: `www.cosmo-model.org`)

COSMO Newsletters

No. 1: February 2001.
No. 2: February 2002.
No. 3: February 2003.
No. 4: February 2004.
No. 5: April 2005.
No. 6: July 2006; Proceedings from the COSMO General Meeting 2005.
No. 7: May 2008; Proceedings from the COSMO General Meeting 2006.
No. 8: August 2008; Proceedings from the COSMO General Meeting 2007.
No. 9: December 2008; Proceedings from the COSMO General Meeting 2008.
No.10: January 2010; Proceedings from the COSMO General Meeting 2009.
No.11: February 2011; Proceedings from the COSMO General Meeting 2010.
No.12: March 2012; Proceedings from the COSMO General Meeting 2011.
No.13: April 2013; Proceedings from the COSMO General Meeting 2012.
No.14: April 2014; Proceedings from the COSMO General Meeting 2013.
No.15: July 2015; Proceedings from the COSMO General Meeting 2014.
No.16: June 2016; Proceedings from the COSMO General Meeting 2015.

COSMO Technical Reports

No. 1: Dmitrii Mironov and Matthias Raschendorfer (2001):
Evaluation of Empirical Parameters of the New LM Surface-Layer Parameterization Scheme. Results from Numerical Experiments Including the Soil Moisture Analysis.

No. 2: Reinhold Schrodin and Erdmann Heise (2001):
The Multi-Layer Version of the DWD Soil Model TERRA_LM.

No. 3: Günther Doms (2001):
A Scheme for Monotonic Numerical Diffusion in the LM.

No. 4: Hans-Joachim Herzog, Ursula Schubert, Gerd Vogel, Adelheid Fiedler and Roswitha Kirchner (2002):
LLM — the High-Resolving Nonhydrostatic Simulation Model in the DWD-Project LITFASS.
Part I: Modelling Technique and Simulation Method.

No. 5: Jean-Marie Bettems (2002):
EUCOS Impact Study Using the Limited-Area Non-Hydrostatic NWP Model in Operational Use at MeteoSwiss.

No. 6: Heinz-Werner Bitzer and Jürgen Steppeler (2004):
Description of the Z-Coordinate Dynamical Core of LM.

No. 7: Hans-Joachim Herzog, Almut Gassmann (2005):
Lorenz- and Charney-Phillips vertical grid experimentation using a compressible nonhydrostatic toy-model relevant to the fast-mode part of the 'Lokal-Modell'

No. 8: Chiara Marsigli, Andrea Montani, Tiziana Paccagnella, Davide Sacchetti, André Walser, Marco Arpagaus, Thomas Schumann (2005):
Evaluation of the Performance of the COSMO-LEPS System

No. 9: Erdmann Heise, Bodo Ritter, Reinhold Schrodin (2006):
Operational Implementation of the Multilayer Soil Model

No. 10: M.D. Tsyrulnikov (2007):
Is the particle filtering approach appropriate for meso-scale data assimilation?

No. 11: Dmitrii V. Mironov (2008):
Parameterization of Lakes in Numerical Weather Prediction. Description of a Lake Model.

No. 12: Adriano Raspanti (2009):
Final report on priority project VERSUS (VERification System Unified Survey).

No. 13: Chiara Mirsigli (2009):
Final report on priority project SREPS (Short Range Ensemble Prediction System).

No. 14: Michael Baldauf (2009):
COSMO Priority Project "Further Developments of the Runge-Kutta Time Integration Scheme" (RK); Final Report.

No. 15: Silke Dierer (2009):
COSMO Priority Project "Further Developments of the Runge-Kutta Time Integration Scheme" (RK); Final Report.

No. 16: Pierre Eckert (2009):
COSMO Priority Project "INTERP"; Final Report.

No. 17: D. Leuenberger, M. Stoll, A. Roches (2010):
Description of some convective indices, implemented in the COSMO model.

No. 18: Daniel Leuenberger (2010):
Statistical Analysis of high-resolution COSMO Ensemble forecasts, in view of Data Assimilation.

No. 19: A. Montani, D. Cesari, C. Marsigli, T. Paccagnella (2010):
Seven years of activity in the field of mesoscale ensemble forecasting by the COSMO-LEPS system: main achievements and open challenges.

No. 20: A. Roches, O. Fuhrer (2012):
Tracer module in the COSMO model.

No. 21: M. Baldauf (2013):
A new fast-waves solver for the Runge-Kutta dynamical core.

No. 22: C. Marsigli, T. Diomede, A. Montani, T. Paccagnella, P. Louka, F. Gofa, A. Corigliano (2013):
The CONSENS Priority Project.

No. 23: M. Baldauf, O. Fuhrer, M. J. Kurowski, G. de Morsier, M. Muellner, Z. P. Piotrowski, B. Rosa, P. L. Vitagliano, D. Wojcik, M. Ziemianski (2013):
The COSMO Priority Project 'Conservative Dynamical Core' Final Report.

No. 24: A. K. Miltenberger, A. Roches, S. Pfahl, H. Wernli (2014):
Online Trajectory Module in COSMO: A short user guide.

No. 25: P. Khain, I. Carmona, A. Voudouri, E. Avgoustoglou, J.-M. Bettems, F. Grazzini (2015):
The Proof of the Parameters Calibration Method: CALMO Progress Report.

No. 26: D. Mironov, E. Machulskaya, B. Szintai, M. Raschendorfer, V. Perov, M. Chumakov, E. Avgoustoglou (2015):
The COSMO Priority Project 'UTCS' Final Report.

No. 27: Jean-Marie Bettems (2015):
The COSMO Priority Project 'COLOBOC' Final Report.

No. 28: Ulrich Blahak (2016):
RADAR_MIE_LM and RADAR_MIELIB - Calculation of Radar Reflectivity from Model Output.